

A CELL-CENTERED FINITE ELEMENT METHOD WITH IMPOSED FLUX CONTINUITY AND STREAMLINE UPWIND TECHNIQUE FOR ADVECTION-DIFFUSION PROBLEMS ON GENERAL MESHES

ONG THANH HAI*, NGUYEN T. HONG THAI, AND TRAN THIEN THANH

Abstract. We extend the cell-centered finite element method (CCFE) [1] with imposed flux continuity and streamline upwind technique to solve the advection-diffusion equations with anisotropic and heterogeneous diffusivity and a convection-dominated regime on general meshes. The scheme is cell-centered in the sense that the solution is computed by cell unknowns of the primal mesh. From general meshes, the method is constructed by the dual meshes and their triangular submeshes. The scheme gives auxiliary edge unknowns interpolated by the multipoint fluid approximation technique to obtain the local continuity of numerical fluxes across the interfaces. In addition, the scheme uses piecewise linear functions combined with a streamline upwind technique on the dual submesh in order to stabilize the numerical solutions and eliminate the spurious oscillations. The coercivity, the strong and dual consistency, and the convergence properties of this method are shown in the rigorous theoretical framework. Numerical results are carried out to highlight accuracy and computational cost.

Key words. Advection-diffusion equations, anisotropic and heterogeneous diffusion, convection-dominated regime, cell-centered schemes, and convergence analysis.

1. Introduction

Many mathematical models involving Partial Differential Equations (PDEs) with both advection and diffusion terms play a fundamental role in solving complicated problems such as various fluid flow, Navier-Stokes equations, etc. The advection-diffusion problems, determined by two physical mechanisms: advection and diffusion, still pose many challenges in finding numerical solutions, especially when the diffusion is anisotropic (*e.g.* tensor-valued) and heterogeneous (*e.g.* nonsmooth, possibly with discontinuities) combined with strongly dominant convection.

On the one hand, one can hardly obtain the approximate solution which converges to the weak one for some general problems with a heterogeneous and anisotropic tensor, possibly with large discontinuities. In fact, when it comes to the discontinuous diffusion problems with the convective term, their approximate solutions computed by the standard finite element method (FEM) can be inaccurate [2]. The authors of [3] proposed a cell-centered scheme, *e.g.* the standard finite volume method (FVM), to address this issue; however, it requires admissible meshes as computational grids [4]. The multi-point flux approximation methods (MPFA) that are also cell-centered schemes precisely approximate the solutions by imposing the local conservation of fluxes [5, 6]. Nevertheless, the MPFA methods only satisfy the coercivity under suitable conditions on the mesh and the permeability tensor. In [7], the authors represented a MUSCL-like cell-centered finite volume method to

Received by the editors on March 6, 2024 and, accepted on December 10, 2024.

2000 *Mathematics Subject Classification.* 65N12, 65N30, 76R05, 76R50.

*Corresponding author.

approximate the solution of multi-dimensional steady advection-diffusion equations, but only for the diffusion process driven by the scalar viscosity field in $C^1(\bar{\Omega})$, not a tensor (possibly with discontinuous). Furthermore, a variety of efficient hybrid numerical schemes have been developed in the last decade to approximate solutions of diffusive equations on general grids, for example, the hybrid mimetic (HM) method [8, 9], the discontinuous Galerkin (DG) method [10, 11], the mimetic finite-difference (MFD) method [12], the mixed finite volume (MFV) method [13], the hybrid finite volume (HFV) method [8], and the discrete duality finite volume method (DDFV) [14]. However, these hybrid methods must depend on more than two different types of unknowns including edges, vertices, and cell ones. This can result in much greater computational cost in the implementation. Therefore, these methods need to rely on condensation arguments (such as Schur complement reduction [15], domain decomposition [16]) in order to reduce the size of the linear systems that need to be solved.

On the other hand, when the problems are isotropic diffusion and convection-dominated, their solutions possess interior and boundary layers. These boundary layers are small subregions where the derivatives of the solution are very large. The widths of these layers are usually significantly smaller than the mesh size, which means the layers are not properly resolved. This leads to unwanted spurious (nonphysical) oscillations in the numerical solution analyzed in [17]. The classical Galerkin formulation is inappropriate for the advection-diffusion problems since, in the case of dominant convection, the discrete solution is usually globally polluted by spurious oscillations, which causes a severe loss of accuracy and stability. To overcome this challenge, according to [9], there are two possible approaches for the convection-diffusion problems. The first approach is that the diffusive term is approximated, and then some forms of centered or upwind approximation of the convection term are implemented to discretize the boundary problems [18, 19, 20]. For the second approach, the total flux of both diffusive and convective terms is approximated, which seems more popular in the finite-element practitioner community. Due to the stability properties and higher-order accuracy, [21] commented that the streamline upwind/ Petrov-Galerkin (SUPG) method developed by Brooks and Hughes [22] is regarded as one of the most efficient procedures for solving convection-dominated equations.

In addition, for the convection-diffusion-reactions equations with a symmetric and uniformly positive definite dispersion-diffusion matrix, the finite volume element methods considered in [23] are based on a Petrov-Galerkin formulation in which the solution space consists of continuous piecewise polynomial functions and the test space consists of piecewise constant functions. This choice of test space is essential for preserving the local conservation property of the method. However, these methods are only implemented on triangular primal meshes, since their piecewise linear finite element spaces are defined on triangulations of the domain; furthermore, they are not cell-centered schemes.

In this paper, we propose a numerical method, namely cell-centered finite element (CCFE), to solve the advection-diffusion problems. This results in addressing two aforementioned challenges due to several following advantages:

1. In the case of heterogeneous and anisotropic diffusivity, possibly with discontinuities, the scheme uses a first-order finite approximation space for the solution and multi-point flux approximations for the discrete gradients to satisfy the local continuity of fluxes. In addition, the scheme adds a streamline upwind diffusion term developed by Brooks and Hughes [22] to

substantially eliminate almost all the difficulties such as spurious crosswind diffusion, non-consistent formulations for the convection-dominated regime. Note that the SDCCFE method in [24] also added a streamline upwind diffusion term, but its discrete gradients (similar to the standard finite element method) do not satisfy flux continuity. This is a key difference from the proposed scheme.

2. Based on the construction of dual meshes and dual sub-meshes, the method is thus suitable for general meshes since it does not deteriorate when the mesh becomes distorted.
3. These dual meshes and dual sub-meshes are constructed in a way that they recover a cell-centered scheme (in which the number of unknowns is the number of elements). Hence, the scheme gives higher accuracy while the computational cost is the same as other cell-centered schemes.
4. The rigorous convergence analysis of the scheme is shown by the coercivity, the strong and dual consistency.
5. The scheme is easily implemented since standard finite element codes relying on triangular meshes are used directly.

The rest of this paper is organized as follows: Section 2 presents the advection-diffusion model with the heterogeneous and anisotropic diffusion tensor and its convection-dominated regime. We represent the discretizations (the meshes, a projection operator, and a discrete gradient) using the CCFE scheme and construct the associated system of linear equations involving only cell unknowns. Section 3 verifies the existence of unique solution of the linear system. We also show the convergence analysis of the CCFE scheme, that is, the coercivity, the strong and dual consistency properties. Numerical experiments, including comparisons with performances of other discretization schemes, are presented in Section 4. These results also illustrate the benefits of using the CCFE method to approximate the advection-diffusion equations with the heterogeneous and anisotropic diffusivity and its convection-dominated regime. Finally, Section 5 concludes the paper.

2. The advection-diffusion problems

2.1. The mathematical model. Let Ω be a bounded, open, connected and polygonal domain in \mathbb{R}^2 with boundary $\partial\Omega$. We consider the advection-diffusion equation

$$(1) \quad -\operatorname{div}(\Lambda \nabla u) + \mathbf{b} \cdot \nabla u + \mu u = f \quad \text{in } \Omega,$$

$$(2) \quad u = 0 \quad \text{on } \partial\Omega,$$

under the following assumptions:

- (A₁) An anisotropic and heterogeneous diffusion tensor $\Lambda \in (L^\infty(\Omega))^{2 \times 2}$ is symmetric and positive definite. There exists two positive constant λ_1, λ_2 such that

$$\lambda_2 |\xi|^2 \geq \Lambda \xi \cdot \xi \geq \lambda_1 |\xi|^2, \quad \text{for all } \xi \in \mathbb{R}^2, \text{ and a.e. } \mathbf{x} \in \Omega.$$

- (A₂) $\mathbf{b} \in [W^{1,\infty}(\Omega)]^2$ and $\mu \in L^\infty(\Omega)$ satisfy $\mu - \frac{1}{2} \operatorname{div} \mathbf{b} \geq \mu_0 > 0$ a.e in Ω .

- (A₃) $f \in L^2(\Omega)$ is a source term.

The weak formulation of (1) consists of finding $\bar{u} \in H_0^1(\Omega)$ such that

$$(3) \quad \int_{\Omega} \left[\begin{array}{c} (\Lambda \nabla \bar{u}) \cdot \nabla v + \frac{1}{2} (\mathbf{b} \cdot \nabla \bar{u}) v \\ -\frac{1}{2} \bar{u} (\mathbf{b} \cdot \nabla v) + \left(\mu - \frac{1}{2} \operatorname{div} \mathbf{b} \right) \bar{u} v \end{array} \right] d\mathbf{x} = \int_{\Omega} f v d\mathbf{x}, \quad \forall v \in H_0^1(\Omega).$$

Owing to the assumptions (A_1) - (A_3) and the Lax-Milgram theorem, the result in [25] established the well-posedness of (3).

2.2. The meshes. The CCFE method is an extension of the cell-centered finite element scheme for stationary diffusion problems [1] to the case of convection-diffusion problems with locally small, heterogeneous and anisotropic diffusivity. Let us begin to construct three meshes: the primal mesh \mathfrak{T}_h , the dual mesh \mathfrak{T}_h^* , and the dual sub-mesh \mathfrak{T}_h^{**} . The construction of these meshes is briefly recalled in the following part of this section.

Firstly, we consider the primal mesh \mathfrak{T}_h that consists of nonempty connected close disjoint subsets of Ω , and have the following interpretation

$$\bar{\Omega} = \bigcup_{K \in \mathfrak{T}_h} K,$$

where K is a star-shaped polygon. In each element $K \in \mathfrak{T}_h$, we choose a point $C_K \in \operatorname{int}(K)$ which is a primary control point of volume K . These points are called as the mesh points of \mathfrak{T}_h . The collection of these mesh points is called \mathfrak{C}_h .

Secondly, to assemble the dual mesh \mathfrak{T}_h^* , we assume that the line segment connecting two mesh points of any two neighbouring elements is inside the domain Ω . Since the construction of the dual mesh \mathfrak{T}_h^* is based on the primary mesh \mathfrak{T}_h , each mesh point of \mathfrak{T}_h^* corresponds to a vertex of \mathfrak{T}_h . The set of vertices in \mathfrak{T}_h is denoted by

$$\mathcal{N} = \{P : P \text{ is a vertex of element } K \in \mathcal{V}\}.$$

And for each $P \in \mathcal{N}$, we also denote by

$$\mathfrak{T}_P = \{K \in \mathfrak{T}_h : K \text{ shares the node } P\},$$

the set of primal elements which contain the node P . There are two cases in which the dual mesh is established (see Figure 1):

- (i) If P is an interior node, then the dual control volume M_P associated with the node P is created by connecting the two mesh points of two neighbouring elements in \mathfrak{T}_P .
- (ii) If the node P is on the boundary $\partial\Omega$, we denote by $e \subset \partial E$ and $\hat{e} \subset \partial \hat{E}$ the two edges on the boundary that have P as their node ($E, \hat{E} \in \mathfrak{T}_P$ could be two different neighbouring elements or just one element). Then, the dual control volume M_P is formed by joining the mesh points of each element E and \hat{E} with the midpoints of e and \hat{e} , respectively. Note that P is also a node of the dual control volume M_P in this case.

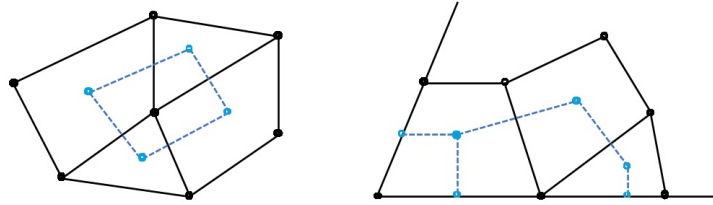


FIGURE 1. Dual control volumes (dashed blue lines) for interior (left) and boundary (right) nodes of the primal mesh \mathfrak{T}_h (solid black lines).

Thus, the dual mesh \mathfrak{T}_h^* can be defined by the collection of all M_P :

$$\bar{\Omega} = \bigcup_{P \in \mathcal{N}} M_P.$$

We also denote by C_{M_P} the mesh point of each dual control volume $M \in \mathfrak{T}_h^*$ which is chosen to be the corresponding vertex P of the primal mesh, *i.e.*

$$(4) \quad C_{M_P} \equiv P, \quad \text{for all } M_P \in \mathfrak{T}_h^*.$$

In the following part of this paper, by dropping the subscript P , this point is written in the simple form C_M . We also denote by \mathfrak{C}_h^* a set of all dual mesh points C_M , $\forall M \in \mathfrak{T}_h^*$.

Finally, we construct the dual sub-mesh \mathfrak{T}_h^{**} as a triangular subgrid of the dual mesh. In particular, for each element $M \in \mathfrak{T}_h^*$, the elements of \mathfrak{T}_h^{**} (denoted by T) associated with M are defined by connecting the dual control point C_M to all nodes of M (see Figure 2).

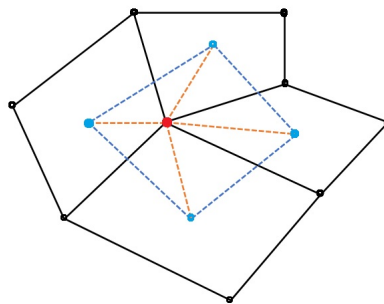


FIGURE 2. The primal mesh \mathfrak{T}_h (solid black lines), its dual mesh \mathfrak{T}_h^* (dashed blue lines), and its dual submesh \mathfrak{T}_h^{**} (dashed red lines).

Hence, we obtain the interpretation as follows:

$$\bar{\Omega} = \bigcup_{T \in \mathfrak{T}_h^{**}} \bar{T}.$$

Note that for all interior triangular elements $T \in \mathfrak{T}_h^{**}$ (*i.e.* $\partial T \cap \partial\Omega = \emptyset$) there exist at least two primal elements $K, L \in \mathfrak{T}_h$ satisfying $T \cap K \neq \emptyset$ and $T \cap L \neq \emptyset$.

Let us denote by \mathcal{N}_Ω^{**} and $\mathcal{N}_{\partial\Omega}^{**}$ the set of interior and boundary nodes of Ω , respectively. Mathematically, \mathcal{N}_Ω^{**} contains the mesh points of primal elements and dual control volumes, that is,

$$(5) \quad \mathcal{N}_\Omega^{**} = \mathfrak{C} \cup \mathfrak{C}^*,$$

where $\mathfrak{C} := \{C_K, \forall K \in \mathfrak{T}_h\}$ and $\mathfrak{C}^* := \{C_M, \forall M \in \mathfrak{T}_h^*\}$. Then, the set of vertices of \mathfrak{T}_h^{**} is defined by

$$(6) \quad \mathcal{N}^{**} = \mathcal{N}_\Omega^{**} \cup \mathcal{N}_{\partial\Omega}^{**}.$$

We also define the size of discretization as follows:

$$(7) \quad h = \sup \{h_T, T \in \mathfrak{T}_h^{**}\},$$

where h_T denotes the diameter of T .

On each primal element $K \in \mathfrak{T}_h$, we denote by $\Lambda_K = \frac{1}{m_K} \int_K \Lambda d\mathbf{x}$ the average of tensor Λ on K , where m_K is the measure of K . For the heterogeneous and anisotropic case, Λ may be discontinuous across two different primal elements, that is,

$$(8) \quad \Lambda_K \neq \Lambda_L \quad \text{for any } K, L \in \mathfrak{T}_h, K \neq L.$$

The CCFE scheme is based on the idea of standard finite element on the triangular dual sub-mesh \mathfrak{T}_h^{**} . In particular, we find an approximate solution of (1) by computing its values at all nodes P of the dual sub-mesh \mathcal{N}^{**} . For this work, let us define by

$$\mathcal{H}_h := \{u_h = (u_P)_{P \in \mathcal{N}^{**}}, u_P \in \mathbb{R}\},$$

the set of all vectors $u_h := (u_P)_{P \in \mathcal{N}^{**}}$, where u_P is an approximate value of the solution u at a node $P \in \mathcal{N}^{**}$. By (5), each vector u_h can be rewritten as

$$u_h = (u_P)_{P \in \mathcal{N}^{**}} = \left((u_K)_{K \in \mathfrak{T}_h}, (u_M)_{M \in \mathfrak{T}_h^*}, (u_P)_{P \in \mathcal{N}_\Omega^{**}} \right)^t,$$

where u_K and u_M are two approximate values of u at nodes C_K and C_M , respectively.

Due to the homogeneous Dirichlet boundary condition, we need to define a subset \mathcal{H}_h^0 of \mathcal{H}_h by

$$\mathcal{H}_h^0 = \{u_h \in \mathcal{H}_h : u_P = 0 \forall P \in \mathcal{N}_{\partial\Omega}^{**}\}.$$

2.3. The projection operator and the discrete gradient. In this section, we introduce a projection operator Πu_h and the discrete gradient $\nabla_\Lambda u_h$ for any $u_h \in \mathcal{H}_h$ to write the discrete form of variational problem (3). These two operators should be defined by their restrictions to each triangular element T of \mathfrak{T}_h^{**} . Based on the properties of tensor Λ , these definitions are represented in the two following cases:

For the case of isotropic tensor Λ , we seek Πu_h of the form

$$(9) \quad \Pi u_h|_T = \sum_{P \in \mathcal{N}_T^{**}} u_P L_P(\mathbf{x}),$$

where \mathcal{N}_T^{**} is the set of three vertices of T and L_P is a first-order Lagrange basis function associated with a vertex P .

Since the function $\Pi u_h|_T$ belongs to $H^1(T)$, a restriction of the discrete gradient on T is defined by

$$(10) \quad \nabla_\Lambda u_h|_T = \nabla \Pi u_h(\mathbf{x}), \quad \text{a.e. } \mathbf{x} \in T.$$

For the case of anisotropic and heterogeneous tensor Λ , we consider a triangle $T = (C_M, C_K, C_L)$ in \mathfrak{T}_h^* , where K, L are two primal elements of \mathfrak{T}_h , and M is a dual control volume of \mathfrak{T}_h^* (see Figure 3). There has a common edge e between K

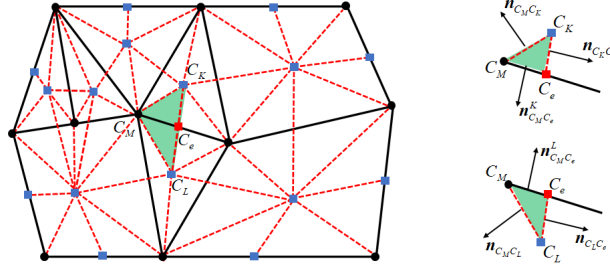


FIGURE 3. Left: A triangular element (green) $T = (C_M, C_K, C_L)$ of the dual submesh \mathfrak{T}_h^* ; Right: Outward normal vectors of two sub-triangles of T .

and L . This edge intersects the segment $C_K C_L$ at a point C_e . Thus, the triangle T can be partitioned into two sub-triangles $T_1 = (C_M C_e C_K)$ and $T_2 = (C_M C_e C_L)$. In addition, we denote by $\mathbf{n}_{C_M C_e}^K$, $\mathbf{n}_{C_M C_K}$ and $\mathbf{n}_{C_K C_e}$ the outward normal vectors of the triangle T_1 whose lengths are equal to the segments $C_M C_e$, $C_M C_K$ and $C_K C_e$, respectively. The notation m_{T_1} is the measure of triangle T_1 . Note that $\mathbf{n}_{C_M C_e}^K + \mathbf{n}_{C_M C_e}^L = 0$.

Next, we introduce an auxiliary unknown u_e^M , which is an approximation of u at C_e seeing from M . Remark that if e is a boundary edge, then u_e^M is equal to 0 because of the homogenous Dirichlet boundary condition (2).

For any vector $u_h \in \mathcal{H}_h$, the function $\Pi u_h|_T$ is continuous on T , and piecewise linear on each T_1 and T_2 . Both the projection operator $\Pi u_h|_T$ and the discrete gradient $\nabla_\Lambda u_h|_T$ must be taken into account the tensor Λ and defined as follows

(i) On the triangle T_1 , we have

$$(11) \quad \Pi u_h|_{T_1}(\mathbf{x}) = \begin{cases} u_K & \text{if } \mathbf{x} = C_K, \\ u_M & \text{if } \mathbf{x} = C_M, \\ u_e^M & \text{if } \mathbf{x} = C_e. \end{cases}$$

By the multi-point flux approximations, we define the restriction of $\nabla_\Lambda u_h$ on T_1 as

$$(12) \quad \nabla_\Lambda u_h|_{T_1} = \frac{-u_e^M \mathbf{n}_{C_M C_K} - u_K \mathbf{n}_{C_M C_e}^K - u_M \mathbf{n}_{C_K C_e}}{2m_{T_1}}.$$

Similarly, the restriction of Πu_h and $\nabla_\Lambda u_h$ on the triangle T_2 are also defined as

$$(13) \quad \Pi u_h|_{T_2}(\mathbf{x}) = \begin{cases} u_L & \text{if } \mathbf{x} = C_L, \\ u_M & \text{if } \mathbf{x} = C_M, \\ u_e^M & \text{if } \mathbf{x} = C_e, \end{cases}$$

and

$$(14) \quad \nabla_\Lambda u_h|_{T_2} = \frac{-u_e^M \mathbf{n}_{C_M C_L} - u_L \mathbf{n}_{C_M C_e}^L - u_M \mathbf{n}_{C_L C_e}}{2m_{T_2}}.$$

(ii) Next, we determine the auxiliary unknown u_e^M to strongly satisfy the following total flux conservation at the internal edge $C_M C_e$

$$(15) \quad \int_{C_M C_e} (\Lambda_K \nabla_{\Lambda} u_h|_{T_1}) \cdot \mathbf{n}_{C_M C_e}^K + (\Lambda_L \nabla_{\Lambda} u_h|_{T_2}) \cdot \mathbf{n}_{C_M C_e}^L d\gamma = 0.$$

With the assumption of

$$(16) \quad \Delta = \frac{(\mathbf{n}_{C_M C_e}^K)^t \Lambda_K \mathbf{n}_{C_M C_K}}{2m_{T_1}} + \frac{(\mathbf{n}_{C_M C_e}^L)^t \Lambda_L \mathbf{n}_{C_M C_L}}{2m_{T_2}} \neq 0,$$

we calculate (15) to get the following linear combination of the auxiliary unknown u_e^M

$$(17) \quad u_e^M = \beta_K^{M,e} u_K + \beta_L^{M,e} u_L + \beta_M^{M,e} u_M,$$

with

$$\begin{aligned} \beta_K^{M,e} &= -\frac{1}{\Delta} \frac{(\mathbf{n}_{C_M C_e}^K)^t \Lambda_K \mathbf{n}_{C_M C_e}^K}{2m_{T_1}}, \\ \beta_L^{M,e} &= -\frac{1}{\Delta} \frac{(\mathbf{n}_{C_M C_e}^L)^t \Lambda_L \mathbf{n}_{C_M C_e}^L}{2m_{T_2}}, \\ \beta_M^{M,e} &= 1 - \beta_K^{M,e} - \beta_L^{M,e}, \end{aligned}$$

in which \mathbf{n}^t is the tranpose of vector \mathbf{n} .

Remark 2.1. *It is easy to satisfy (16) by moving slightly locations of primal mesh points.*

Substituting (17) into (12) and (14), we deduce that the restrictions of the function Πu_h and the discrete gradient $\nabla_{\Lambda} u_h$ on $T = (C_M C_K C_L) \in \mathfrak{T}_h^{**}$ linearly depend on the three values u_M , u_K and u_L :

$$(18) \quad \nabla_{\Lambda} u_h|_{T_1} = -\frac{\tilde{\mathbf{n}}_K^{T_1} u_K + \tilde{\mathbf{n}}_L^{T_1} u_L + \tilde{\mathbf{n}}_M^{T_1} u_M}{2m_{T_1}},$$

$$(19) \quad \nabla_{\Lambda} u_h|_{T_2} = -\frac{\tilde{\mathbf{n}}_K^{T_2} u_K + \tilde{\mathbf{n}}_L^{T_2} u_L + \tilde{\mathbf{n}}_M^{T_2} u_M}{2m_{T_2}},$$

with

$$\begin{aligned} \tilde{\mathbf{n}}_K^{T_1} &= \left(\beta_K^{M,e} \mathbf{n}_{C_M C_K} + \mathbf{n}_{C_M C_e}^K \right), \quad \tilde{\mathbf{n}}_L^{T_1} = \left(\beta_L^{M,e} \mathbf{n}_{C_M C_K} \right), \\ \tilde{\mathbf{n}}_M^{T_1} &= \left(\beta_M^{M,e} \mathbf{n}_{C_M C_K} + \mathbf{n}_{C_K C_e} \right), \quad \tilde{\mathbf{n}}_K^{T_2} = \left(\beta_K^{M,e} \mathbf{n}_{C_M C_L} \right), \\ \tilde{\mathbf{n}}_L^{T_2} &= \left(\beta_L^{M,e} \mathbf{n}_{C_M C_L} + \mathbf{n}_{C_M C_e}^L \right), \quad \tilde{\mathbf{n}}_M^{T_2} = \left(\beta_M^{M,e} \mathbf{n}_{C_M C_L} + \mathbf{n}_{C_L C_e} \right). \end{aligned}$$

Remark 2.2. *For any $M, \widehat{M} \in \mathfrak{T}_h^*$ such that $e = C_M C_{\widehat{M}}$ is an internal edge of the primal mesh, there are two values of solution at C_e , one from M (u_e^M), and another from \widehat{M} ($u_e^{\widehat{M}}$). As (17) for u_e^M , we also have that $u_e^{\widehat{M}}$ can be represented as a linear combination of $u_{\widehat{M}}$, u_K and u_L . Since two adjacent triangles (C_M, C_K, C_L) and $(C_{\widehat{M}}, C_K, C_L)$ are distinct, there are two different values of solution at C_e : $u_e^M \neq u_e^{\widehat{M}}$. Note that for the homogeneous Dirichlet boundary condition, if $C_e \in \partial\Omega$, then $u_e^M = u_e^{\widehat{M}} = 0$.*

Using the above definitions, we write the following discrete form of (3): finding $u_h \in \mathcal{H}_h^0$ such that for all $v_h \in \mathcal{H}_h^0$,

$$(20) \quad \int_{\Omega} \left[\begin{array}{c} (\Lambda \nabla_{\Lambda} u_h) \cdot \nabla_{\Lambda} v_h + \frac{1}{2} (\mathbf{b} \cdot \nabla_{\Lambda} u_h) \Pi v_h \\ -\frac{1}{2} \Pi u_h (\mathbf{b} \cdot \nabla_{\Lambda} v_h) + \left(\mu - \frac{1}{2} \operatorname{div} \mathbf{b} \right) \Pi u_h \Pi v_h \end{array} \right] d\mathbf{x} = \int_{\Omega} f \Pi v_h d\mathbf{x}.$$

In the dominated convection situations, the Galerkin method lacks stability to find the approximate solutions for the advection-diffusion problems. Having said that, the CCFE scheme also lacks stability since it inherits a basis of the standard finite element method (FEM). Thus, to improve the stability of CCFE scheme, we add the streamline upwind term in (20) as follows:

$$(21) \quad \begin{aligned} & \int_{\Omega} (\Lambda \nabla_{\Lambda} u_h) \cdot \nabla_{\Lambda} v_h d\mathbf{x} + \frac{1}{2} \int_{\Omega} (\mathbf{b} \cdot \nabla_{\Lambda} u_h) \Pi v_h d\mathbf{x} - \frac{1}{2} \int_{\Omega} (\mathbf{b} \cdot \nabla_{\Lambda} v_h) \Pi u_h d\mathbf{x} \\ & + \int_{\Omega} \left(\mu - \frac{1}{2} \operatorname{div} \mathbf{b} \right) \Pi u_h \Pi v_h d\mathbf{x} + \sum_{T \in \mathfrak{T}_h^{**}} \delta_T \int_T (\mathbf{b} \cdot \nabla_{\Lambda} u_h + \mu \Pi u_h) (\mathbf{b} \cdot \nabla_{\Lambda} v_h) d\mathbf{x} \\ & = \sum_{T \in \mathfrak{T}_h^{**}} \int_T \delta_T f (\mathbf{b} \cdot \nabla_{\Lambda} v_h) d\mathbf{x} + \int_{\Omega} f \Pi v_h d\mathbf{x}, \quad \forall v_h \in \mathcal{H}_h^0. \end{aligned}$$

In (21), for every $T \in \mathfrak{T}_h^{**}$, the stabilization parameter δ_T taken from [21, Eq.(5)], that is,

$$(22) \quad \delta_T = \frac{h_T}{2 \|\mathbf{b}\|_{(W^{1,\infty}(T))^2}} \xi(\operatorname{Pe}_T), \quad \text{with } \operatorname{Pe}_T = \frac{\|\mathbf{b}\|_{(W^{1,\infty}(T))^2} h_T}{2\lambda_T},$$

where ξ is an upwind function (such that $\frac{\xi(\alpha)}{\alpha}$ is bounded for $\alpha \rightarrow 0+$) and Pe_T is the local Péclet number. Here, we set

$$(23) \quad \lambda_T = \begin{cases} \min(1, \operatorname{spec}(\Lambda_K), \operatorname{spec}(\Lambda_L)) & \text{if } T \cap K \neq \emptyset \text{ and } T \cap L \neq \emptyset, \text{ with } K, L \in \mathfrak{T}_h, \\ \min(1, \operatorname{spec}(\Lambda_K)) & \text{otherwise, with } T \subset K, \text{ and } K \in \mathfrak{T}_h, \end{cases}$$

where $\operatorname{spec}(\Lambda_K)$ are the eigenvalues of Λ_K .

2.4. The linear algebraic system. For each $Q \in \mathcal{N}_{\Omega}^{**}$, we choose v_h in (20) and

$$(21) \text{ by } e_h^Q = (e_P^Q)_{P \in \mathcal{N}^{**}} \in \mathcal{H}_h^0 \text{ such that } e_P^Q = \begin{cases} 1 & \text{if } P = Q, \\ 0 & \text{if } P \neq Q. \end{cases}$$

Since $u_h = \sum_{P \in \mathcal{N}_{\Omega}^{**}} u_P e_h^P$, $\nabla_{\Lambda} u_h = \sum_{P \in \mathcal{N}_{\Omega}^{**}} u_P \nabla_{\Lambda} e_h^P$ and $\Pi u_h = \sum_{P \in \mathcal{N}_{\Omega}^{**}} u_P \Pi e_h^P$, we can rewrite (20) by

$$(24) \quad \begin{aligned} & \sum_{P \in \mathcal{N}_{\Omega}^{**}} u_P \sum_{T \in \mathfrak{T}_h^{**}} \int_T \left[\begin{array}{c} (\Lambda \nabla_{\Lambda} e_h^P) \cdot \nabla_{\Lambda} e_h^Q + \frac{1}{2} (\mathbf{b} \cdot \nabla_{\Lambda} e_h^P) \Pi e_h^Q \\ -\frac{1}{2} \Pi e_h^P (\mathbf{b} \cdot \nabla_{\Lambda} e_h^Q) \\ + \left(\mu - \frac{1}{2} \operatorname{div} \mathbf{b} \right) \Pi e_h^P \Pi e_h^Q \end{array} \right] d\mathbf{x} \\ & = \sum_{T \in \mathfrak{T}_h^{**}} \int_T f \Pi e_h^Q d\mathbf{x}, \end{aligned}$$

and (21) by

$$(25) \quad \sum_{P \in \mathcal{N}_{\Omega}^{**}} u_P \sum_{T \in \mathfrak{T}_h^{**}} \int_T \left[\begin{array}{l} (\Lambda \nabla_{\Lambda} e_h^P) \cdot \nabla_{\Lambda} e_h^Q + \frac{1}{2} (\mathbf{b} \cdot \nabla_{\Lambda} e_h^P) \Pi e_h^Q \\ - \frac{1}{2} \Pi e_h^P (\mathbf{b} \cdot \nabla_{\Lambda} e_h^Q) + \left(\mu - \frac{1}{2} \operatorname{div} \mathbf{b} \right) \Pi e_h^P \Pi e_h^Q \\ + \delta_T [\mathbf{b} \cdot \nabla_{\Lambda} e_h^P + \mu \Pi e_h^P] (\mathbf{b} \cdot \nabla_{\Lambda} e_h^Q) \end{array} \right] d\mathbf{x} \\ = \sum_{T \in \mathfrak{T}_h^{**}} \int_T \left[f \Pi e_h^Q + \delta_T f (\mathbf{b} \cdot \nabla_{\Lambda} e_h^Q) \right] d\mathbf{x}.$$

Next, we denote by \mathfrak{T}_P^{**} a set of all triangular elements of \mathfrak{T}_h^{**} having a common vertex P . By the construction of dual mesh \mathfrak{T}_h^* , for any $M \in \mathfrak{T}_h^*$, it follows that all elements of $\mathfrak{T}_{C_M}^{**}$ are inside M . This means two compact support sets of the function $\Pi e_h^{C_M}$ and the discrete gradient $\nabla_{\Lambda} e_h^{C_M}$ are also inside M . With these compact supports, the set of interior nodes of M (denoted by \mathcal{N}_M^{**}) is defined by

$$(26) \quad \mathcal{N}_M^{**} = C_M \cup \mathfrak{C}_M,$$

where $\mathfrak{C}_M = \{C_K \in \mathfrak{C} : K \cap M \neq \emptyset\}$.

In order to derive the linear algebraic system associated with (20) and (21), we implement the following computational process:

(a) For each $M \in \mathfrak{T}_h^*$, by taking $v_h = e_h^{C_M}$ into (20) and (21), and from (26), we obtain the following equation

$$(27) \quad D_{MM} u_M + \sum_{K \in \mathfrak{C}_M} E_{MK} u_K = F_M^*,$$

where coefficients D_{MM} , E_{MK} and F_M^* are computed from (24):

$$D_{MM} = \sum_{T \in \mathfrak{T}_{C_M}^{**}} \int_T \left[(\Lambda \nabla_{\Lambda} e_h^{C_M}) \cdot \nabla_{\Lambda} e_h^{C_M} + \left(\mu - \frac{1}{2} \operatorname{div} \mathbf{b} \right) \Pi e_h^{C_M} \Pi e_h^{C_M} \right] d\mathbf{x}, \\ E_{MK} = \sum_{T \in (\mathfrak{T}_{C_K}^{**} \cap \mathfrak{T}_{C_M}^{**})} \int_T \left[\begin{array}{l} (\Lambda \nabla_{\Lambda} e_h^{C_K}) \cdot \nabla_{\Lambda} e_h^{C_M} + \left(\mu - \frac{1}{2} \operatorname{div} \mathbf{b} \right) \Pi e_h^{C_K} \Pi e_h^{C_M} \\ + \frac{1}{2} (\mathbf{b} \cdot \nabla_{\Lambda} e_h^{C_K}) \Pi e_h^{C_M} - \frac{1}{2} \Pi e_h^{C_K} (\mathbf{b} \cdot \nabla_{\Lambda} e_h^{C_M}) \end{array} \right] d\mathbf{x}, \\ F_M^* = \int_M f \Pi e_h^{C_M} d\mathbf{x}.$$

From (25), we also have

$$D_{MM} = \sum_{T \in \mathfrak{T}_{C_M}^{**}} \int_T \left[\begin{array}{l} (\Lambda \nabla_{\Lambda} e_h^{C_M}) \cdot \nabla_{\Lambda} e_h^{C_M} + \left(\mu - \frac{1}{2} \operatorname{div} \mathbf{b} \right) (\Pi e_h^{C_M})^2 \\ + \delta_T [\mathbf{b} \cdot \nabla_{\Lambda} e_h^{C_M} + \mu \Pi e_h^{C_M}] (\mathbf{b} \cdot \nabla_{\Lambda} e_h^{C_M}) \end{array} \right] d\mathbf{x}, \\ E_{MK} = \sum_{T \in (\mathfrak{T}_{C_K}^{**} \cap \mathfrak{T}_{C_M}^{**})} \int_T \left[\begin{array}{l} (\Lambda \nabla_{\Lambda} e_h^{C_K}) \cdot \nabla_{\Lambda} e_h^{C_M} + \left(\mu - \frac{1}{2} \operatorname{div} \mathbf{b} \right) \Pi e_h^{C_K} \Pi e_h^{C_M} \\ + \frac{1}{2} (\mathbf{b} \cdot \nabla_{\Lambda} e_h^{C_K}) \Pi e_h^{C_M} - \frac{1}{2} \Pi e_h^{C_K} (\mathbf{b} \cdot \nabla_{\Lambda} e_h^{C_M}) \\ + \delta_T [\mathbf{b} \cdot \nabla_{\Lambda} e_h^{C_K} + \mu \Pi e_h^{C_K}] (\mathbf{b} \cdot \nabla_{\Lambda} e_h^{C_M}) \end{array} \right] d\mathbf{x}, \\ F_M^* = \sum_{T \in \mathfrak{T}_{C_M}^{**}} \int_T f \left[\Pi e_h^{C_M} + \delta_T (\mathbf{b} \cdot \nabla_{\Lambda} e_h^{C_M}) \right] d\mathbf{x}.$$

From (27), if $D_{MM} \neq 0$, then the unknown u_M is represented in the following linear combination

$$(28) \quad u_M = \frac{1}{D_{MM}} \left(F_M^* - \sum_{K \in \mathcal{C}_M} E_{MK} u_K \right).$$

Then, for all $M \in \mathfrak{T}_h^*$, we can write the first linear system as follows

$$(29) \quad \mathbf{D} \mathbf{U}^* + \mathbf{E} \mathbf{U} = \mathbf{F}^*,$$

with $\mathbf{D} = (D_{MM})_{M \in \mathfrak{T}_h^*} \in \mathbb{R}^{\text{card}(\mathfrak{T}_h^*) \times \text{card}(\mathfrak{T}_h^*)}$, $\mathbf{E} = (E_{MK})_{M \in \mathfrak{T}_h^*, K \in \mathfrak{T}_h} \in \mathbb{R}^{\text{card}(\mathfrak{T}_h^*) \times \text{card}(\mathfrak{T}_h)}$, $\mathbf{U}^* = (u_M)_{M \in \mathfrak{T}_h^*} \in \mathbb{R}^{\text{card}(\mathfrak{T}_h^*)}$, $\mathbf{U} = (u_K)_{K \in \mathfrak{T}_h} \in \mathbb{R}^{\text{card}(\mathfrak{T}_h)}$, and $\mathbf{F}^* = (F_M^*)_{M \in \mathfrak{T}_h^*} \in \mathbb{R}^{\text{card}(\mathfrak{T}_h^*)}$.

Note that \mathbf{D} is a diagonal matrix. If all of its diagonal elements are different from zero, (29) leads to

$$(30) \quad \mathbf{U}^* = \mathbf{D}^{-1} (\mathbf{F}^* - \mathbf{E} \mathbf{U}).$$

(b) For each $K \in \mathfrak{T}_h$, by taking $v_h = e_h^{CK} \in \mathcal{H}_h^0$ into (20) and (21), we then write the second linear system:

$$(31) \quad \mathbf{G} \mathbf{U}^* + \mathbf{H} \mathbf{U} = \mathbf{F},$$

with $\mathbf{G} = (G_{KM})_{K \in \mathfrak{T}_h, M \in \mathfrak{T}_h^*} \in \mathbb{R}^{\text{card}(\mathfrak{T}_h) \times \text{card}(\mathfrak{T}_h^*)}$, $\mathbf{H} = (H_{KL})_{K, L \in \mathfrak{T}_h} \in \mathbb{R}^{\text{card}(\mathfrak{T}_h) \times \text{card}(\mathfrak{T}_h)}$ and $\mathbf{F} = (F_K)_{K \in \mathfrak{T}_h} \in \mathbb{R}^{\text{card}(\mathfrak{T}_h)}$. Their coefficients are computed from (24):

$$G_{KM} = \sum_{T \in (\mathfrak{T}_{C_K}^{**} \cap \mathfrak{T}_{C_M}^{**})} \int_T \left[\begin{aligned} & \left(\Lambda \nabla_\Lambda e_h^{CM} \right) \cdot \nabla_\Lambda e_h^{CK} + \left(\mu - \frac{1}{2} \text{div} \mathbf{b} \right) \Pi e_h^{CM} \Pi e_h^{CK} \\ & + \frac{1}{2} (\mathbf{b} \cdot \nabla_\Lambda e_h^{CM}) \Pi e_h^{CK} - \frac{1}{2} \Pi e_h^{CM} (\mathbf{b} \cdot \nabla_\Lambda e_h^{CK}) \end{aligned} \right] d\mathbf{x},$$

$$H_{KL} = \sum_{T \in (\mathfrak{T}_{C_K}^{**} \cap \mathfrak{T}_{C_L}^{**})} \int_T \left[\begin{aligned} & \left(\Lambda \nabla_\Lambda e_h^{CL} \right) \cdot \nabla_\Lambda e_h^{CK} + \left(\mu - \frac{1}{2} \text{div} \mathbf{b} \right) \Pi e_h^{CL} \Pi e_h^{CK} \\ & + \frac{1}{2} (\mathbf{b} \cdot \nabla_\Lambda e_h^{CL}) \Pi e_h^{CK} - \frac{1}{2} \Pi e_h^{CL} (\mathbf{b} \cdot \nabla_\Lambda e_h^{CK}) \end{aligned} \right] d\mathbf{x},$$

$$F_K = \int_\Omega f \Pi e_h^{CK} d\mathbf{x}.$$

From (25), we also get

$$G_{KM} = \sum_{T \in (\mathfrak{T}_{C_K}^{**} \cap \mathfrak{T}_{C_M}^{**})} \int_T \left[\begin{aligned} & \left(\Lambda \nabla_\Lambda e_h^{CM} \right) \cdot \nabla_\Lambda e_h^{CK} + \left(\mu - \frac{1}{2} \text{div} \mathbf{b} \right) \Pi e_h^{CM} \Pi e_h^{CK} \\ & + \frac{1}{2} (\mathbf{b} \cdot \nabla_\Lambda e_h^{CM}) \Pi e_h^{CK} - \frac{1}{2} \Pi e_h^{CM} (\mathbf{b} \cdot \nabla_\Lambda e_h^{CK}) \\ & + \delta_T \left[\mathbf{b} \cdot \nabla_\Lambda e_h^{CM} + \mu \Pi e_h^{CM} \right] (\mathbf{b} \cdot \nabla_\Lambda e_h^{CK}) \end{aligned} \right] d\mathbf{x},$$

$$H_{KL} = \sum_{T \in (\mathfrak{T}_{C_K}^{**} \cap \mathfrak{T}_{C_L}^{**})} \int_T \left[\begin{aligned} & \left(\Lambda \nabla_\Lambda e_h^{CL} \right) \cdot \nabla_\Lambda e_h^{CK} + \left(\mu - \frac{1}{2} \text{div} \mathbf{b} \right) \Pi e_h^{CL} \Pi e_h^{CK} \\ & + \frac{1}{2} (\mathbf{b} \cdot \nabla_\Lambda e_h^{CL}) \Pi e_h^{CK} - \frac{1}{2} \Pi e_h^{CL} (\mathbf{b} \cdot \nabla_\Lambda e_h^{CK}) \\ & + \delta_T \left[\mathbf{b} \cdot \nabla_\Lambda e_h^{CL} + \mu \Pi e_h^{CL} \right] (\mathbf{b} \cdot \nabla_\Lambda e_h^{CK}) \end{aligned} \right] d\mathbf{x},$$

$$F_K = \sum_{T \in \mathfrak{T}_{C_K}^{**}} \int_T f \left[\Pi e_h^{CK} + \delta_T (\mathbf{b} \cdot \nabla_\Lambda e_h^{CK}) \right] d\mathbf{x}.$$

(c) Substituting (30) into (31), we end up with a linear system of the form

$$(32) \quad \mathbf{A} \mathbf{U} = \mathbf{B},$$

where $\mathbf{A} = \mathbf{H} - \mathbf{G} \mathbf{D}^{-1} \mathbf{E} \in \mathbb{R}^{\text{card}(\mathfrak{T}_h) \times \text{card}(\mathfrak{T}_h)}$, $\mathbf{B} = \mathbf{F} - \mathbf{G} \mathbf{D}^{-1} \mathbf{F}^* \in \mathbb{R}^{\text{card}(\mathfrak{T}_h)}$.

Remark 2.3. *Since the matrix \mathbf{A} belongs to $\mathbb{R}^{\text{card}(\mathfrak{T}_h) \times \text{card}(\mathfrak{T}_h)}$, the computational cost for solving (32) is the same as that of other cell-centered schemes.*

3. Mathematical properties

We now show the existence of unique solution of CCFE scheme in (20) or (21) as follows:

Proposition 3.1. *Under Hypothesis $(A_1) - (A_4)$, let \mathcal{D}^* be a discretization, and assume that the coefficient δ_T satisfies*

$$(33) \quad 0 < \delta_T \leq \frac{1}{2} \min \left\{ \frac{h_T^2}{\lambda_2^2 C_{inv}^2}, \frac{\mu_0}{\|\mu\|_{L^\infty(T)}^2} \right\}, \quad \forall T \in \mathfrak{T}_h^{**},$$

where the positive constant C_{inv} is arisen from [26, Theorem C.30 (Inverse estimate), p.745]. Then the problem (32) has a unique solution.

Proof of Proposition 3.1: By combining the systems (29) and (31), we get

$$(34) \quad \widehat{\mathbf{A}} \widehat{\mathbf{U}} = \widehat{\mathbf{F}}$$

where $\widehat{\mathbf{A}} := \begin{pmatrix} \mathbf{D} & \mathbf{E} \\ \mathbf{G} & \mathbf{H} \end{pmatrix}$, $\widehat{\mathbf{U}} := \begin{pmatrix} \mathbf{U} \\ \mathbf{U}^* \end{pmatrix}$ and $\widehat{\mathbf{F}} := \begin{pmatrix} \mathbf{F} \\ \mathbf{F}^* \end{pmatrix}$.

Let define two bilinear forms $a(u_h, u_h)$ and $a_{\text{SU}}(u_h, u_h)$ on \mathcal{H}_h , where $a_{\text{SU}}(u_h, u_h)$ is associated with the dominated-convection regime problem. From two assumptions (A_1) and (A_2) , for any $u_h \neq \mathbf{0}$, we obtain

$$\begin{aligned} a(u_h, u_h) &= \int_{\Omega} \left[(\Lambda \nabla_{\Lambda} u_h) \cdot \nabla_{\Lambda} u_h + \left(\mu - \frac{1}{2} \text{div } \mathbf{b} \right) (\Pi u_h)^2 \right] d\mathbf{x} > 0 \\ a_{\text{SU}}(u_h, u_h) &= \int_{\Omega} (\Lambda \nabla_{\Lambda} u_h) \cdot \nabla_{\Lambda} u_h d\mathbf{x} + \int_{\Omega} \left(\mu - \frac{1}{2} \text{div } \mathbf{b} \right) (\Pi u_h)^2 d\mathbf{x} \\ &\quad + \sum_{T \in \mathfrak{T}_h^{**}} \delta_T \left[\int_T (\mathbf{b} \cdot \nabla_{\Lambda} u_h)^2 d\mathbf{x} + \int_T \mu \Pi u_h (\mathbf{b} \cdot \nabla_{\Lambda} u_h) d\mathbf{x} \right], \\ &\geq \sum_{T \in \mathfrak{T}_{\mathcal{C}_M}^{**}} \int_T \left[(\Lambda \nabla_{\Lambda} u_h) \cdot \nabla_{\Lambda} u_h + \left(\mu - \frac{1}{2} \text{div } \mathbf{b} \right) (\Pi u_h)^2 \right. \\ &\quad \left. + \delta_T (\mathbf{b} \cdot \nabla_{\Lambda} u_h)^2 - \delta_T |\mu \Pi u_h (\mathbf{b} \cdot \nabla_{\Lambda} u_h)| \right] d\mathbf{x}, \\ &\geq \sum_{T \in \mathfrak{T}_{\mathcal{C}_M}^{**}} \int_T \left[(\Lambda \nabla_{\Lambda} u_h) \cdot \nabla_{\Lambda} u_h + \frac{3}{4} \delta_T (\mathbf{b} \cdot \nabla_{\Lambda} u_h)^2 \right] d\mathbf{x} > 0, \end{aligned}$$

due to the assumption (A_2) , the condition (33), and the Cauchy-Schwarz inequality, that is,

$$\begin{aligned} \delta_T \int_T |\mu \Pi u_h (\mathbf{b} \cdot \nabla_{\Lambda} u_h)| d\mathbf{x} &\leq \sqrt{\delta_T} \|\mu\|_{L^\infty(T)} \|\Pi u_h\|_{L^2(T)} \left\| \sqrt{\delta_T} (\mathbf{b} \cdot \nabla_{\Lambda} u_h) \right\|_{L^2(T)}, \\ &\leq \sqrt{\frac{\mu_0}{2}} \|\Pi u_h\|_{L^2(T)} \left\| \sqrt{\delta_T} (\mathbf{b} \cdot \nabla_{\Lambda} u_h) \right\|_{L^2(T)}, \\ &\leq \frac{\mu_0}{2} \|\Pi u_h\|_{L^2(T)}^2 + \frac{1}{4} \left\| \sqrt{\delta_T} (\mathbf{b} \cdot \nabla_{\Lambda} u_h) \right\|_{L^2(T)}^2. \end{aligned}$$

Since $\widehat{\mathbf{U}}^t \widehat{\mathbf{A}} \widehat{\mathbf{U}}$ is associated with $a(u_h, u_h)$ or $a_{\text{SU}}(u_h, u_h)$, we then have

$$(35) \quad \widehat{\mathbf{U}}^t \widehat{\mathbf{A}} \widehat{\mathbf{U}} > 0 \quad \text{for any } \widehat{\mathbf{U}} \neq \mathbf{0}$$

in which $\widehat{\mathbf{U}}^t$ is the tranpose of vector $\widehat{\mathbf{U}}$.

This follows that $\widehat{\mathbf{A}}$ is positive definite.

Moreover, we see that the main diagonal of \mathbf{D} is

$$(36) \quad D_{MM} = \sum_{T \in \mathfrak{T}_{C_M}^{**}} \int_T \left[(\Lambda \nabla_{\Lambda} e_h^{C_M}) \cdot \nabla_{\Lambda} e_h^{C_M} + \left(\mu - \frac{1}{2} \operatorname{div} \mathbf{b} \right) (\Pi e_h^{C_M})^2 \right] d\mathbf{x} > 0,$$

In the dominated-convection regime, we also have

$$(37) \quad \begin{aligned} D_{MM} &= \sum_{T \in \mathfrak{T}_{C_M}^{**}} \int_T \left[(\Lambda \nabla_{\Lambda} e_h^{C_M}) \cdot \nabla_{\Lambda} e_h^{C_M} + \left(\mu - \frac{1}{2} \operatorname{div} \mathbf{b} \right) (\Pi e_h^{C_M})^2 \right. \\ &\quad \left. + \delta_T \left[\mathbf{b} \cdot \nabla_{\Lambda} e_h^{C_M} + \mu \Pi e_h^{C_M} \right] (\mathbf{b} \cdot \nabla_{\Lambda} e_h^{C_M}) \right] d\mathbf{x}, \\ &\geq \sum_{T \in \mathfrak{T}_{C_M}^{**}} \int_T \left[(\Lambda \nabla_{\Lambda} e_h^{C_M}) \cdot \nabla_{\Lambda} e_h^{C_M} + \frac{3}{4} \delta_T (\mathbf{b} \cdot \nabla_{\Lambda} e_h^{C_M})^2 \right] d\mathbf{x} > 0. \end{aligned}$$

According to [27, Theorem 2.1 (i)], the Schur complement $\mathbf{A} = \mathbf{H} - \mathbf{G} \mathbf{D}^{-1} \mathbf{E}$ of \mathbf{D} is invertible, since the matrix \mathbf{D} is positive definite and the positive-definite matrix $\widehat{\mathbf{A}}$ is invertible.

■

We now focus on demonstrating the theoretical convergence of the proposed scheme. For isotropic diffusion tensor Λ without convection-dominated regime, the scheme is equivalent to the standard finite element scheme on the triangular subdual mesh \mathfrak{T}_h^{**} . For isotropic diffusion tensor Λ in convection-dominated regime, its convergence analysis is similar as the streamline upwind Petrov-Galerkin method on the triangular subdual mesh \mathfrak{T}_h^{**} . With the remainder of this work, we show its convergence analysis in the case of heterogeneous, anisotropic or possibly discontinuous tensor Λ in convection-dominated regime. For this purpose, we introduce the following properties: let us define the discretization $\widehat{\mathcal{D}}^{**} = (\mathcal{H}_{\widehat{\mathcal{D}}^{**}}^0, \Pi, \nabla_{\Lambda})$ having

- (i) The coercivity of discretization $\widehat{\mathcal{D}}^{**}$ is measured through the coefficient $C_{\widehat{\mathcal{D}}^{**}}$ of the linear mapping Π defined by

$$(38) \quad C_{\widehat{\mathcal{D}}^{**}} := \max_{\substack{v_h \in \mathcal{H}_h^0 \\ \|v_h\| = 1}} \|\Pi v_h\|_{L^2(\Omega)}.$$

A sequence $(\widehat{\mathcal{D}}_h^{**})_{h \in \mathbb{R}}$ is coercive if there exists $C_{\Pi} > 0$ such that

$$(39) \quad C_{\widehat{\mathcal{D}}_h^{**}} \leq C_{\Pi}, \quad \forall h.$$

- (ii) The strong consistency of discretization $\widehat{\mathcal{D}}^{**}$ is measured through the function $S_{\widehat{\mathcal{D}}^{**}} : H_0^1(\Omega) \rightarrow [0, +\infty)$ defined by

$$(40) \quad \forall \varphi \in H_0^1(\Omega), \quad S_{\widehat{\mathcal{D}}^{**}}(\varphi) := \min_{v_h \in \mathcal{H}_h^0} \left(\|\Pi v_h - \varphi\|_{L^2(\Omega)} + \|\nabla_{\Lambda} v_h - \nabla \varphi\|_{(L^2(\Omega))^2} \right).$$

A sequence $(\widehat{\mathcal{D}}_h^{**})_{h \in \mathbb{R}}$ is strongly consistent if, for all $\varphi \in H_0^1(\Omega)$, $S_{\widehat{\mathcal{D}}_h^{**}}(\varphi)$ tends to 0 as $h \rightarrow 0$.

- (iii) The dual consistency (or limit-conforming) of the discretization $\widehat{\mathcal{D}}^{**}$ is measured through the function $W_{\widehat{\mathcal{D}}^{**}} : (H_0^1(\Omega))^2 \rightarrow [0, +\infty)$ defined by

$$(41) \quad W_{\widehat{\mathcal{D}}^{**}}(\boldsymbol{\varphi}) := \max_{\substack{v_h \in \mathcal{H}_{\widehat{\mathcal{D}}^{**}}^0 \\ \|v_h\| = 1}} \int_{\Omega} [\nabla_{\Lambda} v_h \cdot \boldsymbol{\varphi} + \Pi v_h \operatorname{div} \boldsymbol{\varphi}] d\mathbf{x}, \quad \forall \boldsymbol{\varphi} \in (H_0^1(\Omega))^2.$$

Besides, we define the following discrete H^1 -norm by

$$\|v_h\|_{1,\mathcal{D}^{**}}^2 := \sum_{T \in \mathfrak{T}_h^{**}} \frac{|\mathbf{n}_{KL}|}{d_{KL}} (v_K - v_L)^2 + \frac{|\mathbf{n}_{KM}|}{d_{KM}} (v_K - v_M)^2 + \frac{|\mathbf{n}_{LM}|}{d_{LM}} (v_L - v_M)^2,$$

and the norm $\|\cdot\|$ used for the dominated-convection regime:

$$(42) \quad \|\|v_h\|\|^2 := \lambda_1 \|\nabla_\Lambda v_h\|_{L^2(\Omega)}^2 + \sum_{T \in \mathfrak{T}_h^{**}} \left\| \delta_T^{1/2} (\mathbf{b} \cdot \nabla_\Lambda v_h) \right\|_{L^2(T)}^2,$$

for any $v_h \in \mathcal{H}_h$.

Based on the properties of Λ , \mathfrak{T}_h^{**} is classified into two following sets

$$\begin{aligned} \mathfrak{T}_{h,\Lambda}^{**} &= \{T \in \mathfrak{T}_h^{**} : \Lambda \text{ is not continuous on } T\}, \\ \mathfrak{T}_{h,\text{const}}^{**} &= \{T \in \mathfrak{T}_h^{**} : \Lambda \text{ is constant on } T\}. \end{aligned}$$

If $T \in \mathfrak{T}_{h,\Lambda}^{**}$, let us assume that

$$\Lambda(\mathbf{x}) = \begin{cases} \Lambda_1, & \text{if } \mathbf{x} \in T_1, \\ \Lambda_2, & \text{if } \mathbf{x} \in T_2, \end{cases}$$

where T_1, T_2 are two sub-triangles of T (see Figure 4).

Next, we represent Theorem 3.2 to verify the convergence, *i.e.*

$$(43) \quad \|\nabla \bar{u} - \nabla_\Lambda u_h\|_{(L^2(\Omega))^2} \rightarrow 0, \text{ and } \|\bar{u} - \Pi u_h\|_{L^2(\Omega)} \rightarrow 0, \text{ as } h \rightarrow 0,$$

by showing the strong, dual consistency, and the coercive properties.

Theorem 3.2. *In the dominated-convection situation, under Hypotheses $(A_1) - (A_4)$, let \bar{u} be the unique weak solution (3) of the problem (1), and satisfies the assumption $\Lambda \nabla \bar{u} \in W^{\text{div},2}(\Omega)$. Let consider a discretization $\widehat{\mathcal{D}}^{**}$, we assume that there exists two positive constants, one is C_Π satisfying (62), and another is θ independent of h such that*

$$(44) \quad \max \left\{ \frac{h_T}{h_{T_1}}, \frac{h_T}{h_{T_2}} \right\} \leq \theta, \quad \forall T \in (\mathfrak{T}_h^{**} \setminus \mathfrak{T}_{h,\text{const}}^{**}),$$

Also, the coefficient δ_T defined in (22) satisfies

$$(45) \quad 0 < \delta_T \leq \frac{1}{2} \min \left\{ \frac{h_T^2}{\lambda_2^2 C_{inv}^2}, \frac{\mu_0}{\|\mu\|_{L^\infty(T)}^2} \right\}, \quad \forall T \in \mathfrak{T}_h^{**},$$

where the positive constant C_{inv} is arisen from [26, Theorem C.30 (Inverse estimate), p.745].

Then, there exists a unique solution $u_{\mathcal{D}^{**}} \in \mathcal{H}_h^0$ of the CCFE scheme (21) and a positive constant Θ depends on $\Lambda, \mathbf{b}, \mu, \mu_0$ and θ , such that

$$(46) \quad \begin{aligned} &\|\bar{u} - \Pi u_{\mathcal{D}^{**}}\|_{L^2(\Omega)} + \|\nabla \bar{u} - \nabla_\Lambda u_{\mathcal{D}^{**}}\|_{(L^2(\Omega))^2} \\ &\leq \Theta [W_{\mathcal{D}^{**}}(\Lambda \nabla \bar{u}) + W_{\mathcal{D}^{**}}(-\mathbf{b}\bar{u}) + S_{\mathcal{D}^{**}}(\bar{u})]. \end{aligned}$$

Remark that, the proof is not straightforward from [28, Theorem 3.1], since the proposed method adds to the original bilinear form a term which is a suitable amount of artificial viscosity in the direction of streamlines.

Proof of Theorem 3.2: With $\Lambda \nabla \bar{u} \in W^{\text{div},2}(\Omega)$, we can insert $\varphi = \Lambda \nabla \bar{u}$ in (41), and implement $\text{div}(\Lambda \nabla \bar{u}) = \mathbf{b} \cdot \nabla \bar{u} + \mu \bar{u} - f$ a.e. Ω to rewrite

$$(47) \quad W_{\mathcal{D}^{**}}(\Lambda \nabla \bar{u}) = \max_{\substack{v_h \in \mathcal{H}_h^0 \\ \|v_h\|=1}} \int_{\Omega} [(\Lambda \nabla \bar{u}) \cdot \nabla_{\Lambda} v_h + (\mathbf{b} \cdot \nabla \bar{u}) \Pi v_h + \mu \bar{u} \Pi v_h - f \Pi v_h] d\mathbf{x}.$$

Moreover, if we choose $\varphi = -\mathbf{b}\bar{u}$ for (41), then it follows

$$(48) \quad \int_{\Omega} [\nabla_{\Lambda} v_h \cdot (\mathbf{b}\bar{u}) + \Pi v_h \text{div}(\mathbf{b}\bar{u})] d\mathbf{x} \geq -W_{\mathcal{D}^{**}}(-\mathbf{b}\bar{u}), \quad \forall v_h \in \mathcal{H}_h^0.$$

In (47), we replace $-\int_{\Omega} f \Pi v_h d\mathbf{x}$ with the remainder of (21) and $-\text{div}(\Lambda \nabla \bar{u}) + \mathbf{b} \cdot \nabla \bar{u} + \mu \bar{u} = f$ a.e. Ω to obtain the following estimation

$$(49) \quad \begin{aligned} & \|v_h\| W_{\mathcal{D}^{**}}(\Lambda \nabla \bar{u}) \\ & \geq \int_{\Omega} \left[(\Lambda \nabla \bar{u} - \Lambda \nabla_{\Lambda} u_{\mathcal{D}^{**}}) \cdot \nabla_{\Lambda} v_h + \frac{1}{2} \mathbf{b} \cdot (\nabla \bar{u} - \nabla_{\Lambda} u_{\mathcal{D}^{**}}) \Pi v_h \right] d\mathbf{x} \\ & \quad + \frac{1}{2} \int_{\Omega} (\mathbf{b} \cdot \nabla_{\Lambda} v_h) (\Pi u_{\mathcal{D}^{**}} - \bar{u}) d\mathbf{x} + \frac{1}{2} \int_{\Omega} [(\mathbf{b} \cdot \nabla_{\Lambda} v_h) \bar{u} + \text{div}(\mathbf{b}\bar{u}) \Pi v_h] d\mathbf{x} \\ & \quad + \frac{1}{2} \int_{\Omega} \text{div} \mathbf{b} (\Pi u_{\mathcal{D}^{**}} - \bar{u}) \Pi v_h d\mathbf{x} + \int_{\Omega} \mu (\bar{u} - \Pi u_{\mathcal{D}^{**}}) \Pi v_h d\mathbf{x} \\ & \quad + \sum_{T \in \mathfrak{T}_h^{**}} \delta_T \int_T [\mathbf{b} \cdot (\nabla \bar{u} - \nabla_{\Lambda} u_{\mathcal{D}^{**}}) + \mu (\bar{u} - \Pi u_{\mathcal{D}^{**}})] (\mathbf{b} \cdot \nabla_{\Lambda} v_h) d\mathbf{x} \\ & \quad - \sum_{T \in \mathfrak{T}_{h,\text{const}}^{**}} \delta_T \int_T \text{div} [\Lambda \nabla \bar{u} - \Lambda_T (\nabla_{\Lambda} u_{\mathcal{D}^{**}})|_T] (\mathbf{b} \cdot \nabla_{\Lambda} v_h)|_T d\mathbf{x} \\ & \quad - \sum_{\substack{T \in (\mathfrak{T}_h^{**} \setminus \mathfrak{T}_{h,\text{const}}^{**}) \\ T := (C_K, C_L, C_M)}} \delta_T \left[\int_{T_1} \text{div} [\Lambda \nabla \bar{u} - \Lambda_{T_1} (\nabla_{\Lambda} u_{\mathcal{D}^{**}})|_{T_1}] (\mathbf{b} \cdot \nabla_{\Lambda} v_h)|_{T_1} d\mathbf{x} \right. \\ & \quad \left. + \int_{T_2} \text{div} [\Lambda \nabla \bar{u} - \Lambda_{T_2} (\nabla_{\Lambda} u_{\mathcal{D}^{**}})|_{T_2}] \mathbf{b} \cdot (\nabla_{\Lambda} v_h)|_{T_2} d\mathbf{x} \right]. \end{aligned}$$

Let us define $I_{\mathcal{D}^{**}} : H_0^1(\Omega) \rightarrow \mathcal{H}_h^0$ by

$$(50) \quad I_{\mathcal{D}^{**}} \varphi := \arg \min_{v_h \in \mathcal{H}_h^0} \left(\|\Pi v_h - \varphi\|_{L^2(\Omega)} + \|\nabla_{\Lambda} v_h - \nabla \varphi\|_{(L^2(\Omega))^2} \right)$$

to insert $-I_{\mathcal{D}^{**}} \bar{u} + I_{\mathcal{D}^{**}} \bar{u}$ into each term of the right hand side of (49). And by invoking (48) for $\int_{\Omega} [\text{div}(\mathbf{b}\bar{u}) \Pi v_h + (\mathbf{b}\bar{u}) \cdot \nabla_{\Lambda} v_h] d\mathbf{x}$ in (49), it leads to the following inequality

$$(51) \quad \|v_h\| W_{\mathcal{D}^{**}}(\Lambda \nabla \bar{u}) + \|v_h\| W_{\mathcal{D}^{**}}(-\mathbf{b}\bar{u}) \geq I_1(\bar{u}, I_{\mathcal{D}^{**}} \bar{u}, v_h) + I_2(I_{\mathcal{D}^{**}} \bar{u}, \Pi u_{\mathcal{D}^{**}}, v_h),$$

where

$$\begin{aligned}
I_1(\bar{u}, I_{\widehat{\mathcal{D}}^{**}}\bar{u}, v_h) &:= \int_{\Omega} (\Lambda \nabla \bar{u} - \Lambda \nabla_{\Lambda} I_{\widehat{\mathcal{D}}^{**}}\bar{u}) \cdot \nabla_{\Lambda} v_h \, d\mathbf{x} \\
&+ \frac{1}{2} \int_{\Omega} \mathbf{b} \cdot (\nabla \bar{u} - \nabla_{\Lambda} I_{\widehat{\mathcal{D}}^{**}}\bar{u}) \Pi v_h \, d\mathbf{x} \\
&+ \frac{1}{2} \int_{\Omega} (\mathbf{b} \cdot \nabla_{\Lambda} v_h) (\Pi I_{\widehat{\mathcal{D}}^{**}}\bar{u} - \bar{u}) \, d\mathbf{x} + \frac{1}{2} \int_{\Omega} \operatorname{div} \mathbf{b} (\Pi I_{\widehat{\mathcal{D}}^{**}}\bar{u} - \bar{u}) \Pi v_h \, d\mathbf{x} \\
&+ \int_{\Omega} \mu (\bar{u} - \Pi I_{\widehat{\mathcal{D}}^{**}}\bar{u}) \Pi v_h \, d\mathbf{x} + \sum_{T \in \mathfrak{T}_h^{**}} \delta_T \int_T \mu (\bar{u} - \Pi I_{\widehat{\mathcal{D}}^{**}}\bar{u}) (\mathbf{b} \cdot \nabla_{\Lambda} v_h) \, d\mathbf{x} \\
&+ \sum_{T \in \mathfrak{T}_h^{**}} \delta_T \int_T [\mathbf{b} \cdot (\nabla \bar{u} - \nabla_{\Lambda} I_{\widehat{\mathcal{D}}^{**}}\bar{u})] (\mathbf{b} \cdot \nabla_{\Lambda} v_h) \, d\mathbf{x} \\
&- \sum_{T \in \mathfrak{T}_h^{**}, \text{const}} \delta_T \int_T \operatorname{div} [\Lambda \nabla \bar{u} - \Lambda_T (\nabla_{\Lambda} I_{\widehat{\mathcal{D}}^{**}}\bar{u})|_T] (\mathbf{b} \cdot \nabla_{\Lambda} v_h)|_T \, d\mathbf{x} \\
&- \sum_{\substack{T \in (\mathfrak{T}_h^{**} \setminus \mathfrak{T}_h^{**}, \text{const}) \\ T := (C_K, C_L, C_M)}} \delta_T \left[\int_{T_1} \operatorname{div} [\Lambda \nabla \bar{u} - \Lambda_{T_1} (\nabla_{\Lambda} I_{\widehat{\mathcal{D}}^{**}}\bar{u})|_{T_1}] (\mathbf{b} \cdot \nabla_{\Lambda} v_h)|_{T_1} \, d\mathbf{x} \right. \\
&\quad \left. + \int_{T_2} \operatorname{div} [\Lambda \nabla \bar{u} - \Lambda_{T_2} (\nabla_{\Lambda} I_{\widehat{\mathcal{D}}^{**}}\bar{u})|_{T_2}] (\mathbf{b} \cdot \nabla_{\Lambda} v_h)|_{T_2} \, d\mathbf{x} \right],
\end{aligned}$$

and

$$\begin{aligned}
I_2(I_{\widehat{\mathcal{D}}^{**}}\bar{u}, \Pi u_{\widehat{\mathcal{D}}^{**}}, v_h) &= \int_{\Omega} (\Lambda \nabla_{\Lambda} I_{\widehat{\mathcal{D}}^{**}}\bar{u} - \Lambda \nabla_{\Lambda} u_{\widehat{\mathcal{D}}^{**}}) \cdot \nabla_{\Lambda} v_h \, d\mathbf{x} \\
&+ \frac{1}{2} \int_{\Omega} \mathbf{b} \cdot (\nabla_{\Lambda} I_{\widehat{\mathcal{D}}^{**}}\bar{u} - \nabla_{\Lambda} u_{\widehat{\mathcal{D}}^{**}}) \Pi v_h \, d\mathbf{x} - \frac{1}{2} \int_{\Omega} (\mathbf{b} \cdot \nabla_{\Lambda} v_h) (\Pi I_{\widehat{\mathcal{D}}^{**}}\bar{u} - \Pi u_{\widehat{\mathcal{D}}^{**}}) \, d\mathbf{x} \\
&- \frac{1}{2} \int_{\Omega} \operatorname{div} \mathbf{b} (\Pi I_{\widehat{\mathcal{D}}^{**}}\bar{u} - \Pi u_{\widehat{\mathcal{D}}^{**}}) \Pi v_h \, d\mathbf{x} + \int_{\Omega} \mu (\Pi I_{\widehat{\mathcal{D}}^{**}}\bar{u} - \Pi u_{\widehat{\mathcal{D}}^{**}}) \Pi v_h \, d\mathbf{x} \\
&+ \sum_{T \in \mathfrak{T}_h^{**}} \delta_T \int_T [\mathbf{b} \cdot (\nabla_{\Lambda} I_{\widehat{\mathcal{D}}^{**}}\bar{u} - \nabla_{\Lambda} u_{\widehat{\mathcal{D}}^{**}})] (\mathbf{b} \cdot \nabla_{\Lambda} v_h) \, d\mathbf{x} \\
&+ \sum_{T \in \mathfrak{T}_h^{**}} \delta_T \int_T \mu (\Pi I_{\widehat{\mathcal{D}}^{**}}\bar{u} - \Pi u_{\widehat{\mathcal{D}}^{**}}) (\mathbf{b} \cdot \nabla_{\Lambda} v_h) \, d\mathbf{x},
\end{aligned}$$

since the vectors $\Lambda_T (\nabla_{\Lambda} I_{\widehat{\mathcal{D}}^{**}}\bar{u})|_T$, $\Lambda_T (\nabla_{\Lambda} u_{\widehat{\mathcal{D}}^{**}})|_T$, $(\Lambda_{T_i} \nabla_{\Lambda} I_{\widehat{\mathcal{D}}^{**}}\bar{u})$, and $(\Lambda_{T_i} \nabla_{\Lambda} u_{\widehat{\mathcal{D}}^{**}})$ for $i = 1, 2$, are constant vectors.

For $I_1(\bar{u}, I_{\widehat{\mathcal{D}}^{**}}\bar{u}, v_h)$, we apply [26, Theorem C.30, pp.745] and the assumption (A_1) to estimate its following term

$$\begin{aligned}
&\int_{T_i} \operatorname{div} (\Lambda \nabla \bar{u} - \Lambda_{T_i} \nabla_{\Lambda} I_{\widehat{\mathcal{D}}^{**}}\bar{u}) (\mathbf{b} \cdot \nabla_{\Lambda} v_h) \, d\mathbf{x}, \\
&\geq - \|\operatorname{div} (\Lambda \nabla \bar{u} - \Lambda_{T_i} \nabla_{\Lambda} I_{\widehat{\mathcal{D}}^{**}}\bar{u})\|_{L^2(T_i)} \|\mathbf{b} \cdot \nabla_{\Lambda} v_h\|_{L^2(T_i)} \\
(52) \quad &\geq - \frac{C_{\text{inv}}}{h_{T_i}} \lambda_2 \|\nabla \bar{u} - \nabla_{\Lambda} I_{\widehat{\mathcal{D}}^{**}}\bar{u}\|_{L^2(T_i)} \|\mathbf{b} \cdot \nabla_{\Lambda} v_h\|_{L^2(T_i)}.
\end{aligned}$$

Owing to the inequality (52) and the definitions of $S_{\mathcal{D}^{**}}(\bar{u})$ and $I_{\mathcal{D}^{**}}\bar{u}$, the term $I_1(\bar{u}, I_{\hat{\mathcal{D}}^{**}}\bar{u}, v_h)$ be bounded by

$$(53) \quad \begin{aligned} & |I_1(\bar{u}, I_{\hat{\mathcal{D}}^{**}}\bar{u}, v_h)| \\ & \leq S_{\hat{\mathcal{D}}^{**}}(\bar{u}) \left[\begin{aligned} & \frac{\lambda_2}{\sqrt{\lambda_1}} + \frac{1}{2} \left(\frac{1}{\sqrt{\lambda_1}} + C_{\Pi} \right) \|\mathbf{b}\|_{(W^{1,\infty}(\Omega))^2} + \sqrt{2}\theta + \frac{1}{\sqrt{2}} \\ & + C_{\Pi} \left\| \mu - \frac{1}{2} \operatorname{div} \mathbf{b} \right\|_{L^\infty(\Omega)} + \sqrt{\frac{\mu_0}{2}} \left(1 + \frac{\|\mathbf{b}\|_{(W^{1,\infty}(\Omega))^2}}{\|\mu\|_{L^\infty(\Omega)}} \right) \end{aligned} \right], \end{aligned}$$

for all $v_h \in \mathcal{H}_{\hat{\mathcal{D}}^{**}}^0$.

From two inequalities (51) and (53), we obtain

$$(54) \quad \begin{aligned} & I_2(I_{\hat{\mathcal{D}}^{**}}\bar{u}, \Pi u_{\hat{\mathcal{D}}^{**}}, v_h) \\ & \leq \|v_h\| \left\{ \begin{aligned} & W_{\hat{\mathcal{D}}^{**}}(\Lambda \nabla \bar{u}) + W_{\hat{\mathcal{D}}^{**}}(-\mathbf{b}\bar{u}) \\ & + S_{\hat{\mathcal{D}}^{**}}(\bar{u}) \left[\begin{aligned} & \frac{\lambda_2}{\sqrt{\lambda_1}} + \frac{1}{2} \left(\frac{1}{\sqrt{\lambda_1}} + C_{\Pi} \right) \|\mathbf{b}\|_{(W^{1,\infty}(\Omega))^2} + \sqrt{2}\theta + \frac{1}{\sqrt{2}} \\ & + C_{\Pi} \left\| \mu - \frac{1}{2} \operatorname{div} \mathbf{b} \right\|_{L^\infty(\Omega)} + \sqrt{\frac{\mu_0}{2}} \left(1 + \frac{\|\mathbf{b}\|_{(W^{1,\infty}(\Omega))^2}}{\|\mu\|_{L^\infty(\Omega)}} \right) \end{aligned} \right] \end{aligned} \right\}. \end{aligned}$$

After inserting $v_h = (I_{\hat{\mathcal{D}}^{**}}\bar{u} - u_{\hat{\mathcal{D}}^{**}})$ in (54), the following term in $I_2(I_{\hat{\mathcal{D}}^{**}}\bar{u}, \Pi u_{\hat{\mathcal{D}}^{**}}, I_{\hat{\mathcal{D}}^{**}}\bar{u} - u_{\hat{\mathcal{D}}^{**}})$ is estimated by

$$(55) \quad \begin{aligned} & \left| \sum_{T \in \mathfrak{T}_h^{**}} \delta_T \int_T [\mu(\Pi I_{\hat{\mathcal{D}}^{**}}\bar{u} - \Pi u_{\hat{\mathcal{D}}^{**}})] (\mathbf{b} \cdot \nabla_{\Lambda}(I_{\hat{\mathcal{D}}^{**}}\bar{u} - u_{\mathcal{D}^{**}})) d\mathbf{x} \right| \\ & \leq \sum_{T \in \mathfrak{T}_h^{**}} \delta_T^{1/2} \|\mu\|_{L^\infty(T)} \int_T |\Pi I_{\hat{\mathcal{D}}^{**}}\bar{u} - \Pi u_{\mathcal{D}^{**}}| \left| \delta_T^{1/2} \mathbf{b} \cdot \nabla_{\Lambda}(I_{\hat{\mathcal{D}}^{**}}\bar{u} - u_{\hat{\mathcal{D}}^{**}}) \right| d\mathbf{x} \\ & \leq \sum_{T \in \mathfrak{T}_h^{**}} \delta_T^{1/2} \|\mu\|_{L^\infty(T)} \|\Pi I_{\hat{\mathcal{D}}^{**}}\bar{u} - \Pi u_{\hat{\mathcal{D}}^{**}}\|_{L^2(T)} \left\| \delta_T^{1/2} \mathbf{b} \cdot \nabla_{\Lambda}(I_{\hat{\mathcal{D}}^{**}}\bar{u} - u_{\hat{\mathcal{D}}^{**}}) \right\|_{L^2(T)} \\ & \leq \sum_{T \in \mathfrak{T}_h^{**}} \sqrt{\frac{\mu_0}{2}} \|\Pi I_{\hat{\mathcal{D}}^{**}}\bar{u} - \Pi u_{\mathcal{D}^{**}}\|_{L^2(T)} \left\| \delta_T^{1/2} \mathbf{b} \cdot \nabla_{\Lambda}(I_{\hat{\mathcal{D}}^{**}}\bar{u} - u_{\mathcal{D}^{**}}) \right\|_{L^2(T)}, \\ & \leq \left(\frac{\mu_0}{2} \|\Pi I_{\hat{\mathcal{D}}^{**}}\bar{u} - \Pi u_{\hat{\mathcal{D}}^{**}}\|_{L^2(\Omega)}^2 + \frac{1}{4} \sum_{T \in \mathfrak{T}_h^{**}} \left\| \delta_T^{1/2} \mathbf{b} \cdot \nabla_{\Lambda}(I_{\hat{\mathcal{D}}^{**}}\bar{u} - u_{\mathcal{D}^{**}}) \right\|_{L^2(T)}^2 \right) \\ & \leq \frac{1}{2} \left(\mu_0 \|\Pi I_{\hat{\mathcal{D}}^{**}}\bar{u} - \Pi u_h\|_{L^2(\Omega)}^2 + \|I_{\hat{\mathcal{D}}^{**}}\bar{u} - u_{\mathcal{D}^{**}}\|^2 \right). \end{aligned}$$

By the inequality (55), the left-hand side of (54) be lower bounded by

$$(56) \quad \begin{aligned} & I_2(I_{\hat{\mathcal{D}}^{**}}\bar{u}, \Pi u_{\hat{\mathcal{D}}^{**}}, I_{\hat{\mathcal{D}}^{**}}\bar{u} - u_{\hat{\mathcal{D}}^{**}}) \geq \|I_{\hat{\mathcal{D}}^{**}}\bar{u} - u_{\hat{\mathcal{D}}^{**}}\|^2 + \mu_0 \|\Pi I_{\hat{\mathcal{D}}^{**}}\bar{u} - \Pi u_{\hat{\mathcal{D}}^{**}}\|_{L^2(\Omega)}^2 \\ & + \left| \sum_{T \in \mathfrak{T}_h^{**}} \delta_T \int_T [\mu(\Pi I_{\hat{\mathcal{D}}^{**}}\bar{u} - \Pi u_{\hat{\mathcal{D}}^{**}})] (\mathbf{b} \cdot \nabla_{\Lambda}(I_{\hat{\mathcal{D}}^{**}}\bar{u} - u_{\mathcal{D}^{**}})) d\mathbf{x} \right| \\ & \geq \frac{1}{2} \left(\mu_0 \|\Pi I_{\hat{\mathcal{D}}^{**}}\bar{u} - \Pi u_{\hat{\mathcal{D}}^{**}}\|_{L^2(\Omega)}^2 + \|I_{\hat{\mathcal{D}}^{**}}\bar{u} - u_{\hat{\mathcal{D}}^{**}}\|^2 \right). \end{aligned}$$

From (54) and (56), they lead to

$$\begin{aligned}
& 2W_{\widehat{\mathcal{D}}^{**}}(\Lambda \nabla \bar{u}) + 2W_{\widehat{\mathcal{D}}^{**}}(-\mathbf{b}\bar{u}) \\
& + 2S_{\widehat{\mathcal{D}}^{**}}(\bar{u}) \left[\begin{array}{l} \frac{\lambda_2}{\sqrt{\lambda_1}} + \frac{1}{2} \left(\frac{1}{\sqrt{\lambda_1}} + C_{\Pi} \right) \|\mathbf{b}\|_{(W^{1,\infty}(\Omega))^2} + \sqrt{2}\theta + \frac{1}{\sqrt{2}} \\ + C_{\Pi} \left\| \mu - \frac{1}{2} \operatorname{div} \mathbf{b} \right\|_{L^{\infty}(\Omega)} + \sqrt{\frac{\mu_0}{2}} \left(1 + \frac{\|\mathbf{b}\|_{(W^{1,\infty}(\Omega))^2}}{\|\mu\|_{L^{\infty}(\Omega)}} \right) \end{array} \right] \\
(57) \quad & + 2(W_{\widehat{\mathcal{D}}^{**}}(\Lambda \nabla \bar{u}) + W_{\widehat{\mathcal{D}}^{**}}(-\mathbf{b}\bar{u})) \geq \|I_{\widehat{\mathcal{D}}^{**}}\bar{u} - u_{\widehat{\mathcal{D}}^{**}}\|.
\end{aligned}$$

In addition, by using the triangle inequality, the definitions (40), (42), (50) and the coercivity (62), we obtain

$$\begin{aligned}
\|\nabla \bar{u} - \nabla_{\Lambda} u_{\widehat{\mathcal{D}}^{**}}\|_{L^2(\Omega)^2} & \leq \|\nabla \bar{u} - \nabla_{\Lambda} I_{\widehat{\mathcal{D}}^{**}}\bar{u}\|_{L^2(\Omega)^2} + \|\nabla_{\Lambda} I_{\widehat{\mathcal{D}}^{**}}\bar{u} - \nabla_{\Lambda} u_{\widehat{\mathcal{D}}^{**}}\|_{L^2(\Omega)^2} \\
(58) \quad & \leq S_{\widehat{\mathcal{D}}^{**}}(\bar{u}) + \frac{1}{\lambda_1} \|I_{\widehat{\mathcal{D}}^{**}}\bar{u} - u_{\widehat{\mathcal{D}}^{**}}\|,
\end{aligned}$$

and

$$\begin{aligned}
\|\bar{u} - \Pi u_{\widehat{\mathcal{D}}^{**}}\|_{L^2(\Omega)} & \leq \|\bar{u} - \Pi I_{\widehat{\mathcal{D}}^{**}}\bar{u}\|_{L^2(\Omega)} + \|\Pi I_{\widehat{\mathcal{D}}^{**}}\bar{u} - \Pi u_{\widehat{\mathcal{D}}^{**}}\|_{L^2(\Omega)} \\
(59) \quad & \leq S_{\widehat{\mathcal{D}}^{**}}(\bar{u}) + C_{\Pi} \|I_{\widehat{\mathcal{D}}^{**}}\bar{u} - u_{\widehat{\mathcal{D}}^{**}}\|.
\end{aligned}$$

Therefore, we verify the inequality (46) from the results (57)-(59), where

$$\Theta = 2 \max \left\{ \begin{array}{l} \left(\frac{1}{\sqrt{\lambda_1}} + C_{\Pi} \right), \\ 1 + \left(\frac{1}{\sqrt{\lambda_1}} + C_{\Pi} \right) \left[\begin{array}{l} \frac{\lambda_2}{\sqrt{\lambda_1}} + \frac{1}{2} \left(\frac{1}{\sqrt{\lambda_1}} + C_{\Pi} \right) \|\mathbf{b}\|_{(W^{1,\infty}(\Omega))^2} \\ + \sqrt{2}\theta + \frac{1}{\sqrt{2}} + C_{\Pi} \left\| \mu - \frac{1}{2} \operatorname{div} \mathbf{b} \right\|_{L^{\infty}(\Omega)} \\ + \sqrt{\frac{\mu_0}{2}} \left(1 + \frac{\|\mathbf{b}\|_{(W^{1,\infty}(\Omega))^2}}{\|\mu\|_{L^{\infty}(\Omega)}} \right) \end{array} \right] \end{array} \right\}.$$

■

Next, instead of proving the coercivity (39), the strong and dual consistencies (40), (41) directly, this work is simplified by checking these properties for the variant form of the CCFE scheme, named the CCFEb scheme. This scheme is described as follows: finding $u_h \in \mathcal{H}_h^0$ such that

$$\begin{aligned}
& \int_{\Omega} (\Lambda \nabla_{\Lambda} u_h) \cdot \nabla_{\Lambda} v_h \, d\mathbf{x} + \frac{1}{2} \int_{\Omega} (\mathbf{b} \cdot \nabla_{\Lambda} u_h) \Pi_1 v_h \, d\mathbf{x} - \frac{1}{2} \int_{\Omega} (\mathbf{b} \cdot \nabla_{\Lambda} v_h) \Pi_1 u_h \, d\mathbf{x} \\
& + \int_{\Omega} \left(\mu - \frac{1}{2} \operatorname{div} \mathbf{b} \right) \Pi_1 u_h \Pi_1 v_h \, d\mathbf{x} + \sum_{T \in \mathfrak{T}_h^{**}} \delta_T \int_T (\mathbf{b} \cdot \nabla_{\Lambda} u_h + \mu \Pi_1 u_h) (\mathbf{b} \cdot \nabla_{\Lambda} v_h) \, d\mathbf{x} \\
(60) \quad & = \sum_{T \in \mathfrak{T}_h^{**}} \int_T \delta_T f (\mathbf{b} \cdot \nabla_{\Lambda} v_h) \, d\mathbf{x} + \int_{\Omega} f \Pi_1 v_h \, d\mathbf{x}, \quad \forall v_h \in \mathcal{H}_h^0,
\end{aligned}$$

where Π_1 is a piecewise polynomial based on the first-order Lagrange basis functions on \mathfrak{T}_h^{**} .

The CCFEb scheme also has the definitions for the coercive, the strong and dual consistency properties as follows: let us define the discretization $\mathcal{D}^{**} = (\mathcal{H}_{\mathcal{D}^{**}}^0, \Pi_1, \nabla_{\Lambda})$ having

- (i) The coercivity of discretization \mathcal{D}^{**} is measured through the coefficient $C_{\mathcal{D}^{**}}$ of the linear mapping Π_1 defined by

$$(61) \quad C_{\mathcal{D}^{**}} := \max_{\substack{v_h \in \mathcal{H}_h^0, \\ \|v_h\|=1}} \|\Pi_1 v_h\|_{L^2(\Omega)}.$$

A sequence $(\mathcal{D}_h^{**})_{h \in \mathbb{R}}$ is coercive if there exists $C_{\Pi_1} > 0$ such that

$$(62) \quad C_{\mathcal{D}_h^{**}} \leq C_{\Pi_1} \quad \forall h.$$

- (ii) The strong consistency of discretization \mathcal{D}^{**} is measured through the function $S_{\mathcal{D}^{**}} : H_0^1(\Omega) \rightarrow [0, +\infty)$ defined by

$$(63) \quad \forall \varphi \in H_0^1(\Omega), \quad S_{\mathcal{D}^{**}}(\varphi) := \min_{v_h \in \mathcal{H}_h^0} \left(\|\Pi_1 v_h - \varphi\|_{L^2(\Omega)} + \|\nabla_\Lambda v_h - \nabla \varphi\|_{(L^2(\Omega))^2} \right).$$

A sequence $(\mathcal{D}_h^{**})_{h \in \mathbb{R}}$ is strongly consistent if, for all $\varphi \in H_0^1(\Omega)$, $S_{\mathcal{D}_h^{**}}(\varphi)$ tends to 0 as $h \rightarrow 0$.

- (iii) The dual consistency (or limit-conforming) of the discretization \mathcal{D}^{**} is measured through the function $W_{\mathcal{D}^{**}} : (H_0^1(\Omega))^2 \rightarrow [0, +\infty)$ defined by

$$(64) \quad W_{\mathcal{D}^{**}}(\boldsymbol{\varphi}) := \max_{\substack{v_h \in \mathcal{H}_{\mathcal{D}^{**}}^0, \\ \|v_h\|=1}} \int_{\Omega} (\nabla_\Lambda v_h \cdot \boldsymbol{\varphi} + \Pi_1 v_h \operatorname{div} \boldsymbol{\varphi}) \, d\mathbf{x}, \quad \forall \boldsymbol{\varphi} \in (H_0^1(\Omega))^2.$$

To simplify checking the coercive (61), the strong and dual consistencies (63), (64), we assume that, for neighboring control volumes, the line joining their primary mesh points intersects their common edge. With the discretization \mathcal{D}^{**} , for each triangular element $T \in \mathfrak{T}_h^{**}$, we connect its center point C_T to three midpoints C_{KL}, C_{KM} and C_{LM} of its edges $[C_K, C_L]$, $[C_K, C_M]$ and $[C_L, C_M]$, respectively. On three edges $[C_{KL}, C_T]$, $[C_{KM}, C_T]$ and $[C_{LM}, C_T]$, we denote by $\mathbf{n}_{L,K}$, $\mathbf{n}_{K,M}$ and $\mathbf{n}_{M,L}$ the orthogonal vectors to these edges, respectively. Moreover, we also denote by \mathbf{n}_K , \mathbf{n}_L , \mathbf{n}_M , \mathbf{n}_e , $\mathbf{n}_{M,1}$, and $\mathbf{n}_{M,2}$ the orthogonal vectors to the edges $[C_L, C_M]$, $[C_K, C_L]$, $[C_K, C_M]$, $[C_M, C_e]$, $[C_K, C_e]$, and $[C_L, C_e]$. Figure 4 illustrates these definitions for any triangular element $T \in \mathfrak{T}_h^{**}$.

Three distances from C_K to $[C_{KL}, C_T]$, from C_L to $[C_{LM}, C_T]$, and from C_M to $[C_{KM}, C_T]$ are denoted by d_{KL} , d_{LM} , and d_{KM} , respectively. Remark that $d_{KL} = d_{LK}$, $d_{LM} = d_{ML}$ and $d_{KM} = d_{MK}$, where d_{LK} , d_{ML} , and d_{MK} are three distances from C_L to $[C_{KL}, C_T]$, from C_M to $[C_{LM}, C_T]$, and from C_K to $[C_{KM}, C_T]$.

We denote by Ai_K , Ai_L , and Ai_M three polygons $(C_K, C_{K,L}, C_T, C_{K,M})$, $(C_L, C_{K,L}, C_T, C_{L,M})$ and $(C_M, C_{K,M}, C_T, C_{L,M})$. For $u_h \in \mathcal{H}_h$, we define a piecewise constant reconstruction $\Pi_{\mathcal{D}^{**}}^0 u_h$ on these polygons as follows:

$$\Pi_{\mathcal{D}^{**}}^0 u_h(\mathbf{x}) := \begin{cases} \Pi_K^0 u_h = u_K, & \mathbf{x} \in Ai_K, \\ \Pi_L^0 u_h = u_L, & \mathbf{x} \in Ai_L, \\ \Pi_M^0 u_h = u_M, & \mathbf{x} \in Ai_M. \end{cases}$$

Note that the CCFEb scheme employs the projection operator $\Pi_1 u_h$ based on first order Lagrange basis functions on the triangular dual sub-mesh \mathfrak{T}_h^{**} . The convergence of this operator is inherited from the standard finite element method. Therefore, in future work, we will focus on analyzing the properties of the discrete gradient..

For this purpose, we firstly recall Lemmas 5.1 and 5.2 of [1]. Since formulas of the

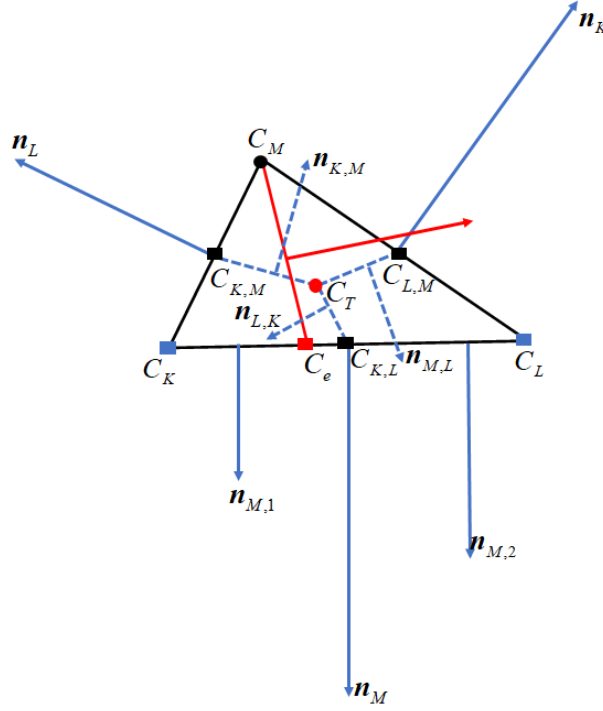


FIGURE 4. A triangular element $T := (C_K, C_L, C_M) \in \mathfrak{T}_h^{**}$ is partitioned into two sub-triangles $T_1 := (C_K, C_e, C_M)$ and $T_2 := (C_L, C_e, C_M)$.

discrete gradients, and the coefficients $\beta_K^{M,e}$, $\beta_L^{M,e}$ and $\beta_M^{M,e}$ are similar as in [1], we have their results as follows:

Lemma 3.3. ([1, Lemma 5.1]) *With assumption (16), let $(\mathcal{D}_m^{**})_{m \in \mathbb{R}}$ be a sequence of discretizations $\mathcal{D}^{**} = (\mathcal{H}_h, h, \Pi_1, \nabla_\Lambda)$ defined. We assume that there exists θ such that*

$$(65) \quad \frac{\min(|\mathbf{n}_{K,L}|, |\mathbf{n}_{K,M}|, |\mathbf{n}_{L,M}|)}{|\mathbf{n}_L|} \frac{m_{T_1}}{m_T} > \theta, \text{ and } \frac{\min(|\mathbf{n}_{K,L}|, |\mathbf{n}_{K,M}|, |\mathbf{n}_{L,M}|)}{|\mathbf{n}_K|} \frac{m_{T_2}}{m_T} > \theta,$$

for all \mathcal{D}_m^{**} , and for $T \in \mathfrak{T}_h^{**} \setminus (\mathfrak{T}_{h,\Lambda}^{**} \cup \mathfrak{T}_{h,\text{const}}^{**})$. Then, for $T \in \mathfrak{T}_h^{**} \setminus \mathfrak{T}_\Lambda^{**}$ and $u_h \in \mathcal{H}_h$, the gradient $\nabla_\Lambda u_h|_T$ satisfies

$$m_T \nabla_\Lambda u_h|_T = (u_M - u_K)(\mathbf{n}_{K,M} + \boldsymbol{\epsilon}_{K,M}) + (u_L - u_M)(\mathbf{n}_{M,L} + \boldsymbol{\epsilon}_{M,L}) + (u_K - u_L)(\mathbf{n}_{L,K} + \boldsymbol{\epsilon}_{L,K}),$$

where there exists three vectors $\boldsymbol{\epsilon}_{K,M}$, $\boldsymbol{\epsilon}_{M,L}$ and $\boldsymbol{\epsilon}_{L,K}$ such that

$$\lim_{h \rightarrow 0} \frac{|\boldsymbol{\epsilon}_{K,M}|}{|\mathbf{n}_{K,M}|} = 0, \quad \lim_{h \rightarrow 0} \frac{|\boldsymbol{\epsilon}_{M,L}|}{|\mathbf{n}_{M,L}|} = 0, \quad \text{and} \quad \lim_{h \rightarrow 0} \frac{|\boldsymbol{\epsilon}_{L,K}|}{|\mathbf{n}_{L,K}|} = 0.$$

Lemma 3.4. ([1, Lemma 5.2]) *With assumption (16), let $(\mathcal{D}_h^{**})_{h \in \mathbb{R}}$ be a sequence of discretizations $\mathcal{D}_h^{**} = (\mathcal{H}_{\mathcal{D}^{**}}^0, h, \Pi_1, \nabla_\Lambda)$ defined. We assume that there exists a positive constant θ independent from h , such that for all \mathcal{D}_h^{**} , for $T \in \mathfrak{T}_\Lambda^{**}$*

$$(H_1) \quad \left| \frac{\mathbf{n}_e^t \Lambda_2 \mathbf{n}_K}{m_{T_2}} - \frac{\mathbf{n}_e^t \Lambda_1 \mathbf{n}_L}{m_{T_1}} \right| \geq \theta \left(\frac{\mathbf{n}_e^t \Lambda_1 \mathbf{n}_e}{m_{T_1}} + \frac{\mathbf{n}_e^t \Lambda_2 \mathbf{n}_e}{m_{T_2}} \right),$$

$$(H_2) \frac{\min \{|\mathbf{n}_{K,L}|, |\mathbf{n}_{K,M}|, |\mathbf{n}_{L,M}|\}}{\max \{|\mathbf{n}_e|, |\mathbf{n}_{M,1}|, |\mathbf{n}_{M,2}|\}} \geq \theta.$$

Then there exists a constant C_2 such that the gradients $\nabla_\Lambda u_h|_{T_1}$ and $\nabla_\Lambda u_h|_{T_2}$ satisfy

$$\begin{aligned} m_{T_1} \nabla_\Lambda u_h|_{T_1} &= (u_M - u_K) \boldsymbol{\theta}_1(K, M) + (u_L - u_M) \boldsymbol{\theta}_1(M, L) + (u_K - u_L) \boldsymbol{\theta}_1(L, K), \\ m_{T_2} \nabla_\Lambda u_h|_{T_2} &= (u_M - u_K) \boldsymbol{\theta}_2(K, M) + (u_L - u_M) \boldsymbol{\theta}_2(M, L) + (u_K - u_L) \boldsymbol{\theta}_2(L, K), \end{aligned}$$

where the vectors $\boldsymbol{\theta}_i(K, M)$, $\boldsymbol{\theta}_i(M, L)$, and $\boldsymbol{\theta}_i(L, K)$ with $i = 1, 2$ satisfy

$$|\boldsymbol{\theta}_i(K, M)| \leq \frac{C_2}{\theta} |\mathbf{n}_{K,M}|, \quad |\boldsymbol{\theta}_i(M, L)| \leq \frac{C_2}{\theta} |\mathbf{n}_{M,L}|, \quad \text{and} \quad |\boldsymbol{\theta}_i(L, K)| \leq \frac{C_2}{\theta} |\mathbf{n}_{L,K}|.$$

Using Lemmas 3.3 and 3.4, it can be shown that the CCFEb scheme exhibits coercivity, duality, and strong consistency properties, similar to the results presented in [1, Proposition 5.3], as follows:

Proposition 3.5. *With assumption (16), let $(\mathcal{D}_h^{**})_{h \in \mathbb{R}}$ be a sequence of discretizations $\mathcal{D}_h^{**} = (\mathcal{H}_{\mathcal{D}^{**}}^0, h, \Pi_1, \nabla_\Lambda)$ defined. We assume that there exists θ , such that for all \mathcal{D}_h^{**} :*

$$\begin{aligned} (H_3) \quad &\rho_T > \theta h_T \text{ for all } T \in \mathfrak{T}_{h, \text{const}}^{**}, \text{ where } \rho_T = \sup\{\text{diam}(S) : S \text{ is a ball} \\ &\quad \text{contained in } T\}, \\ (H_4) \quad &\rho_{T_1} > \theta h_{T_1} \text{ for all } T \in \mathfrak{T}_{h, \text{const}}^{**}, \\ (H_5) \quad &\rho_{T_2} > \theta h_{T_2} \text{ for all } T \in \mathfrak{T}_{h, \text{const}}^{**}, \\ (H_6) \quad &d_{K,L} > \frac{1}{\theta} |\mathbf{n}_{K,L}|, \quad d_{K,M} > \frac{1}{\theta} |\mathbf{n}_{K,M}|, \quad d_{L,M} > \frac{1}{\theta} |\mathbf{n}_{L,M}|, \text{ for all } T \in \mathfrak{T}_h^{**}, \\ (H_7) \quad &\left| \frac{\mathbf{n}_e^t \Lambda_2 \mathbf{n}_K}{m_{T_2}} - \frac{\mathbf{n}_e^t \Lambda_1 \mathbf{n}_L}{m_{T_1}} \right| \geq \theta \left(\frac{\mathbf{n}_\sigma^t \Lambda_1 \mathbf{n}_\sigma}{m_{T_1}} + \frac{\mathbf{n}_\sigma^t \Lambda_2 \mathbf{n}_\sigma}{m_{T_2}} \right) \text{ for all } T \in \mathfrak{T}_{h, \Lambda}^{**}, \\ (H_8) \quad &\frac{\min(|\mathbf{n}_{L,K}|, |\mathbf{n}_{K,M}|, |\mathbf{n}_{M,L}|)}{\max(|\mathbf{n}_e|, |\mathbf{n}_{M,1}|, |\mathbf{n}_{M,2}|)} > \theta, \text{ for all } T \in \mathfrak{T}_{h, \Lambda}^{**}, \\ (H_9) \quad &\frac{\min(|\mathbf{n}_{L,K}|, |\mathbf{n}_{K,M}|, |\mathbf{n}_{M,L}|) m_{T_1}}{|\mathbf{n}_L| m_T} > \theta, \text{ and } \frac{\min(|\mathbf{n}_{L,K}|, |\mathbf{n}_{K,M}|, |\mathbf{n}_{M,L}|) m_{T_2}}{|\mathbf{n}_K| m_T} \\ &> \theta, \text{ for all } T \in \mathfrak{T}_h^{**} \setminus (\mathfrak{T}_{h, \Lambda}^{**} \cup \mathfrak{T}_{h, \text{const}}^{**}) \end{aligned}$$

then the CCFEb scheme is coercive, i.e. there exists $C_{\mathcal{D}^{**}}$ such that

$$(66) \quad \|\Pi_1 u_h\| \leq C_{\mathcal{D}^{**}} \|\nabla_\Lambda u_h\|_{(L^2(\Omega))^2} \leq C_{\mathcal{D}^{**}} \|u_h\|, \quad \forall u_h \in \mathcal{H}_h.$$

Moreover, for all $\varphi \in C_c^\infty(\Omega)$, $\lim_{h \rightarrow 0} S_{\mathcal{D}^{**}}(\varphi) = 0$ and for all $\varphi \in (C_c^\infty(\Omega))^2$ $\lim_{h \rightarrow 0} W_{\mathcal{D}^{**}}(\varphi) = 0$.

Since the spaces $C_c^\infty(\Omega)$ and $(C_c^\infty(\Omega))^2$ are density in $H_0^1(\Omega)$ and $(H_0^1(\Omega))^2$, the CCFEb scheme (60) satisfies the coercive, the dual and strong consistency properties.

4. Numerical experiments

In this section we study a number of examples of problem (1) and (2) with the isotropic and anisotropic heterogeneous diffusion, i.e. continuous and discontinuous diffusive coefficients (subsection 4.1 and 4.2, respectively). The uniform and non-uniform primal meshes are used to compute the solution of each example. To investigate the performance of these discretization methods, we evaluate their convergence rates measured by the absolute error when the meshes are refined. For

this purpose, on each primal mesh \mathfrak{T}_h , we define the absolute error between the exact solution u and the approximate one u_h in the L^2 -norm as follows

$$(67) \quad err_{\mathfrak{T}_h} = \left(\sum_{K \in \mathfrak{T}_h} m_K |u_h(\mathbf{K}) - u(\mathbf{K})|^2 \right)^{\frac{1}{2}},$$

where m_K is the measure of element K of \mathfrak{T}_h .

To discretize our problems, we construct six types of primal meshes in the implementation of our solvers. Fig. 5 illustrates the plots of base meshes of these primal mesh families: the uniform quadrangular mesh (Mesh 1), the uniform triangular mesh (Mesh 2), the distorted quadrangular mesh (Mesh 3) with the distortion density $d = 0.4$, the distorted triangular mesh (Mesh 4) with the distortion density $d = 0.4$, the locally refined non-conforming rectangular mesh (Mesh 5), and the admissible mesh (Mesh 6). These primal meshes are used to discretize the continuous diffusion problems, while the solutions of discontinuous ones are characterized by only Mesh 1 and 6. Each mesh is built based on an $n \times n$ grid. We refine meshes by doubling n and repeating the construction procedure. Note that Mesh 2 (resp. Mesh 6) is constructed by splitting each quadrangle-shaped (resp. quadrilateral-shaped) cell into two triangles. To generate the distorted meshes, i.e. Mesh 3 and 4, we remap the position (x, y) of the nodes of Mesh 1 and 2 into new positions (x', y') through

$$(68) \quad x' = x + r_c d \Delta x,$$

$$(69) \quad y' = y + r_c d \Delta y,$$

where $r_c \in [-1, 1]$ is a random number, $d \in [0, 0.5]$ is a distortion density, Δx and Δy are the sizes of the x and y directions, respectively. Details about the mesh characteristics are reported in Table 1.

TABLE 1. Number of elements of the primal mesh \mathfrak{T}_h in Fig. 5 with the refinement level denoted by p (the base mesh takes $p = 0$).

p	Mesh 1	Mesh 2	Mesh 3	Mesh 4	Mesh 5	Mesh 6
0	16	32	16	32	40	56
1	64	128	64	128	160	224
2	256	512	256	512	640	896
3	1024	2048	1024	2048	2560	3584

4.1. Accuracy. In this subsection, we consider the test case proposed in [9] where the forcing term f in (1) and the inhomogeneous boundary condition function g_D in (2) are set according to their exact solution

$$(70) \quad u(x, y) = \left(x - e^{\frac{2(x-1)}{\nu}} \right) \left(y^2 - e^{\frac{3(y-1)}{\nu}} \right),$$

the coefficients $\mathbf{b} = (2, 3)^T$ and $\mu = 0$, and the domain $\Omega = (0, 1) \times (0, 1)$. Due to the continuity of diffusive coefficient, the diffusion tensor Λ is given by the identity matrix scaled by the positive real factor ν . Moreover, by taking $\nu = 10^{-4}$, our problem becomes strongly convection-dominated and its unknown is defined by an exponential boundary layer near the top and right sides of domain Ω . To deal with this issue, the streamline diffusion cell-centered finite element (SDCCFE) technique [24] is carried out to characterize its solution.

As mentioned in [9] and other references therein, the error measurements include

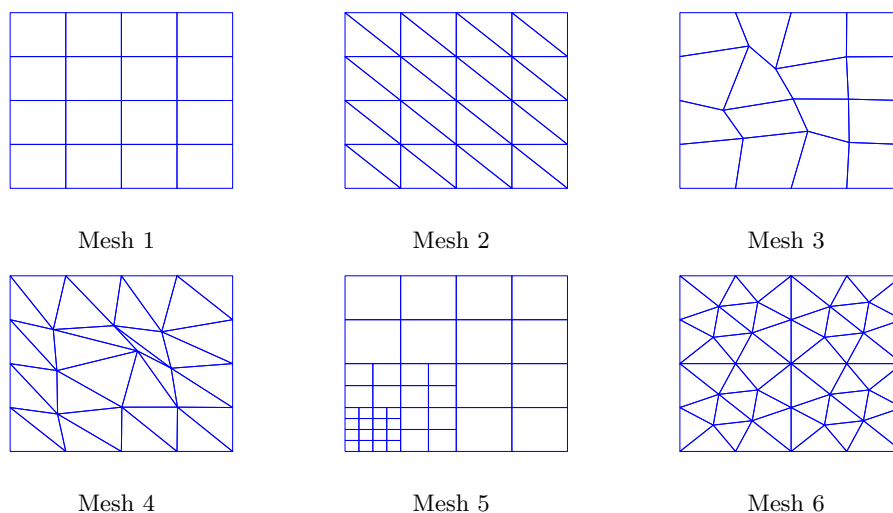


FIGURE 5. Six types of primal meshes are established to discretize the numerical examples: (a) Mesh 1: the uniform quadrangular mesh, (b) Mesh 2: the uniform triangular mesh, (c) Mesh 3: the distorted quadrangular mesh with distortion density $d = 0.4$, (d) Mesh 4: the distorted triangular mesh with distortion density $d = 0.4$, (e) Mesh 5: the locally refined non-conforming rectangular mesh, and (f) Mesh 6: the admissible mesh.

the approximation errors of the solution gradients in the narrow strip around the boundary. This reason may prevent any convergence of the discretization method since these errors are so large. Hence, we restrict our error measurements to the subdomain $[0, 0.95] \times [0, 0.95]$ based on the idea of [9] to avoid these errors. In Table

TABLE 2. Errors of the solutions in L^2 norm and convergence orders of CCFE using six types of primal meshes (see Fig. 5) for the test case with $\nu = 1$.

p	Mesh 1	Mesh 2	Mesh 3	Mesh 4	Mesh 5	Mesh 6
0	6.88e-4	2.54e-4	6.68e-4	2.82e-4	6.34e-4	1.62e-4
1	1.93e-4	7.56e-5	1.96e-4	7.74e-5	1.83e-4	5.83e-5
2	5.20e-5	2.17e-5	5.30e-5	2.23e-5	4.99e-5	1.70e-5
3	1.35e-5	5.84e-6	1.40e-5	6.16e-6	1.30e-5	4.52e-6
Order	1.94	1.89	1.92	1.85	1.94	1.91

2, we show the numerical results of the CCFE method for the case of $\nu = 1$ using six types of primal meshes in Fig. 5. The convergence orders are computed according to the last two rows of the table. These numerical results indicate that the CCFE method exhibits the second order of convergence. Moreover, we observe that the CCFE method delivers better results than other methods in [9] with respect to the error measurements despite their second-order accuracy. Given different numbers of elements in Table 1 and [9, Subsection 4.1, Table 1], the upper plots of [9, Subsection 4.1, Fig. 3] illustrate the minimum values of error measurements are in $(10^{-3}, 10^{-4})$ for the numerical approximation of the exact solution, while those of

the CCFE method are in $(10^{-5}, 10^{-6})$.

In the convection-dominated case, that is, for $\nu = 10^{-4}$, we implement the SDCCFE technique that includes the streamline diffusion term in the CCFE method to tackle our problem, with parameters $\delta_T = \frac{h_T}{2|\mathbf{b}|} \xi(\text{Pe}_T)$, $\xi(\alpha) = \coth \alpha - \frac{1}{\alpha}$ and $\text{Pe}_T = \frac{|\mathbf{b}|h_T}{2\nu}$ for each $T \in \mathfrak{T}_h^{**}$. The numerical results are reported in Table 3 where the last two rows of the table are used to calculate the convergence orders for the CCFE method. We observe that the numerical approximation provided by the CCFE method is first-order accurate. This accuracy is consistent with the error curves displayed in [9, Subsection 4.1, Fig. 3] where the authors present that their methods approximate the exact solution with linear convergence. Note that the domain restriction of error calculations considerably reduces the effects of solution gradients in the narrow strip around the boundary when meshes are refined. Similarly to the diffusive case, the CCFE method yields better numerical approximations than the other methods in [9, Subsection 4.1, Fig. 3]. Given different numbers of elements in Table 1 and [9, Subsection 4.1, Table 1], the values of error measurements obtained by the CCFE method reach 10^{-3} while the other methods in [9, Subsection 4.1, Fig. 3] achieve the minimum results at 10^{-2} . Table 4 shows that the maximum local

TABLE 3. Errors of the solutions in L^2 norm and convergence orders of CCFE using six types of primal meshes (see Fig. 5) with SDCCFE technique for the convection-dominated case ($\nu = 10^{-4}$).

p	Mesh 1	Mesh 2	Mesh 3	Mesh 4	Mesh 5	Mesh 6
0	7.69e-2	5.99e-2	7.41e-2	5.94e-2	8.16e-2	4.05e-2
1	5.05e-2	3.13e-2	4.62e-2	3.33e-2	5.17e-2	2.21e-2
2	2.11e-2	1.61e-2	2.24e-2	1.61e-2	2.02e-2	1.11e-2
3	9.40e-3	7.32e-3	9.70e-3	7.39e-3	8.74e-3	4.68e-3
Order	1.17	1.13	1.21	1.13	1.21	1.24

Pclet numbers, $\text{Pe}_{T^{\max}}$, are in the range $[10^2, 10^4]$. These values are much greater than 1, which is expected for the convection-dominated case ($\nu = 10^{-4}$). However, the associated stabilization parameters $\delta_{T^{\max}}$, are in the range $[10^{-3}, 10^{-1}]$, much smaller than 1. Both $\text{Pe}_{T^{\max}}$ and $\delta_{T^{\max}}$ decrease as the refinement level p increases. This is reasonable, as it helps to reduce the negative impact of the streamline upwind terms on the accuracy of the approximate solution.

4.2. A test case with discontinuous coefficients. In this second test case, we study an example proposed in [29] where the problem (1) and (2) is solved for a discontinuous diffusion tensor and the exact solution is analytically computed. To begin with, the domain $\Omega = [0, 1] \times [0, 1]$ is divided into two subdomains, that is $\Omega = \Omega_1 \cup \Omega_2$, where $\Omega_1 = \left[0, \frac{1}{2}\right] \times [0, 1]$ and $\Omega_2 = \left[\frac{1}{2}, 1\right] \times [0, 1]$. Unlike the isotropic heterogeneous cases in Subsection 4.1, we assume that our diffusion tensor Λ is constant within each subregion, and defined as

$$\Lambda(x, y) = \begin{pmatrix} \lambda(x) & 0 \\ 0 & 1.0 \end{pmatrix},$$

where $\lambda(x)$ is a discontinuous function across the interface $x = \frac{1}{2}$. We denote λ_1 (resp. λ_2) the value of $\lambda(x)$ for $x \in \Omega_1$ (resp. $x \in \Omega_2$). For this test case, we consider

TABLE 4. Maximum local Péclet numbers ($\text{Pe}_{T^{\max}} := \max\{\text{Pe}_T \mid \forall T \in \mathfrak{T}_h^{**}\}$) and associated stabilization parameters ($\delta_{T^{\max}}$) using six types of primal meshes (see Fig. 5) with the refinement level p (see Table 1) for the convection-dominated case ($\nu = 10^{-4}$).

$p = 0$	Mesh 1	Mesh 2	Mesh 3	Mesh 4	Mesh 5	Mesh 6
$\text{Pe}_{T^{\max}}$	5.63e + 3	3.54e + 3	6.04e + 3	4.02e + 3	6.53e + 3	5.56e + 3
$\delta_{T^{\max}}$	4.33e - 3	2.72e - 2	4.65e - 2	3.09e - 2	5.02e - 2	4.27e - 2
$p = 1$	Mesh 1	Mesh 2	Mesh 3	Mesh 4	Mesh 5	Mesh 6
$\text{Pe}_{T^{\max}}$	2.82e + 3	1.77e + 3	3.39e + 3	2.14e + 3	3.27e + 3	2.78e + 3
$\delta_{T^{\max}}$	2.17e - 2	1.36e - 2	2.61e - 2	1.64e - 2	2.51e - 2	2.14e - 2
$p = 2$	Mesh 1	Mesh 2	Mesh 3	Mesh 4	Mesh 5	Mesh 6
$\text{Pe}_{T^{\max}}$	1.41e + 3	8.85e + 2	1.85e + 3	1.14e + 3	1.63e + 3	1.39e + 3
$\delta_{T^{\max}}$	1.08e - 2	6.81e - 3	1.42e - 2	8.78e - 3	1.25e - 2	1.07e - 2
$p = 3$	Mesh 1	Mesh 2	Mesh 3	Mesh 4	Mesh 5	Mesh 6
$\text{Pe}_{T^{\max}}$	7.04e + 2	4.43e + 2	9.26e + 2	5.53e + 2	8.17e + 2	6.95e + 2
$\delta_{T^{\max}}$	5.41e - 3	3.39e - 3	7.12e - 3	4.24e - 3	6.28e - 3	5.34e - 3

three different values of λ_1 , which are 0.1, 5.10^{-2} and 5.10^{-3} , while λ_2 is always set equal to 1.0. By setting $\mathbf{b} = (1, 0)^T$, $\mu = 0$ and $f = 0$, one can easily obtain the exact solution on each subdomain, which is exponential with respect to the x -coordinate and independent of the y -coordinate. The global solution $u(x, y)$ must satisfy the following conditions at the interface between two subregions:

$$\lim_{x \rightarrow \frac{1}{2}^-} u(x, y) = \lim_{x \rightarrow \frac{1}{2}^+} u(x, y), \quad \text{and} \quad \lim_{x \rightarrow \frac{1}{2}^-} -\lambda_1 \partial_x u(x, y) = \lim_{x \rightarrow \frac{1}{2}^+} -\partial_x u(x, y).$$

Letting $u(0, y) = 1$, $u(1, y) = 0$, and applying two matching conditions, we get

$$(71) \quad u\left(\frac{1}{2}, y\right) = \frac{\exp\left(\frac{1}{2\lambda_1}\right)}{1 - \exp\left(\frac{1}{2\lambda_1}\right)} \left(\frac{\exp\left(\frac{1}{2\lambda_1}\right)}{1 - \exp\left(\frac{1}{2\lambda_1}\right)} + \frac{1}{1 - \exp\left(\frac{1}{2}\right)} \right)^{-1}.$$

Consequently, the exact solution in each subdomain can be written as follows

$$(72) \quad u_1(x, y) = \frac{u\left(\frac{1}{2}, y\right) - \exp\left(\frac{1}{2\lambda_1}\right) + (1 - u\left(\frac{1}{2}, y\right)) \exp\left(\frac{x}{\lambda_1}\right)}{1 - \exp\left(\frac{1}{2\lambda_1}\right)},$$

$$(73) \quad u_2(x, y) = \frac{-\exp\left(\frac{1}{2}\right) u\left(\frac{1}{2}, y\right) + u\left(\frac{1}{2}, y\right) \exp\left(x - \frac{1}{2}\right)}{1 - \exp\left(\frac{1}{2}\right)}.$$

To assess the accuracy of the CCFE method for solving the anisotropic heterogeneous diffusion problem, Meshes 1 and 6 are used as primal meshes since they are conforming on the interface $x = \frac{1}{2}$ between Ω_1 and Ω_2 . Furthermore, for the cases where $\lambda_1 = 5.10^{-2}$ or $\lambda_1 = 5.10^{-3}$, the problem on the domain Ω_1 is advection-dominated based on the eigenvalues of Λ (i.e., the Péclet number is consistently large when the eigenvalues of Λ exhibit high contrast). This is due to the calculation of the relative strength of advection over diffusion along the eigenvectors' directions, as detailed in [30, Section 3.3]). Therefore, we implement the SDCCFE

technique, where the streamline diffusion term has parameters $\delta_T = \frac{h_T}{2|\mathbf{b}|}\xi(\text{Pe}_T)$, $\xi(\alpha) = \coth \alpha - \frac{1}{\alpha}$ and $\text{Pe}_T = \frac{|\mathbf{b}|h_T}{2\lambda_1}$ for each $T \in \mathfrak{T}_h^{**}$ that is either inside Ω_1 or intersects with both Ω_1 and Ω_2 .

For convenience in comparing CCFE with other discretization methods in [29], we consider the mesh sizes of each primal mesh family as in Table 5. For the test case

TABLE 5. Mesh-size of Mesh 1 and 6 with respect to the refinement level p .

p	Mesh 1	Mesh 6
0	0.3536	0.2693
1	0.1768	0.1346
2	0.0884	0.0673
3	0.0441	0.0337

with $\lambda_1 = 0.1$, the numerical results are shown in Table 6 where we also calculate the order of convergence according to the last two rows of the table, while a visual comparison is given in Figures 6 and 7. By comparing to the results in [29, Subsection 5.1, Table 1], we deduce that the CCFE scheme exhibits the same orders of convergence as the Symmetric Weighted Interior Penalty (SWIP) method.

TABLE 6. Convergence rates of CCFE method using Mesh 1 and 6 for the case of $\lambda_1 = 0.1$.

p	Mesh 1	Mesh 6
0	7.07e-3	1.55e-2
1	2.74e-3	6.21e-3
2	8.94e-4	2.14e-3
3	2.49e-4	6.49e-4
Order	1.84	1.72

For two numerical examples with $\lambda_1 = 5 \cdot 10^{-2}$ and $\lambda_1 = 5 \cdot 10^{-3}$, we also consider Mesh 1 and 6 characterized by the refinement level $p = 3$ as primal meshes of the CCFE method. In addition to the quantitative analysis measured by the absolute errors in L^2 norm, we introduce the indicator which quantifies overshoots and undershoots of the computed solutions [29] as follows

$$(74) \quad M = \max(|\max_{\Omega}(u_h) - \max_{\Omega}(u)|, |\min_{\Omega}(u_h) - \min_{\Omega}(u)|).$$

The solutions are visualized in Figure 8 (Mesh 1) and 9 (Mesh 6) for $\lambda_1 = 5 \cdot 10^{-2}$, while those for $\lambda_1 = 5 \cdot 10^{-3}$ are displayed in Figures 10 (Mesh 1) and 11 (Mesh 6). The numerical results obtained with $\lambda_1 = 5 \cdot 10^{-2}$ and $\lambda_1 = 5 \cdot 10^{-3}$ are reported in Tables 7. In Table 7, we observe that the CCFE scheme using Mesh 1 and 6 with sufficiently small mesh-sizes performs better than the SWIP and two Interior Penalty (IP) methods in [29, Subsection 5.1, Table 3] with respect to the L^2 -norm errors and the indicator M . Furthermore, with $\lambda_1 = 5 \cdot 10^{-3}$, a comparison of the results in Table 7 with those in [29, Subsection 5.1, Table 4] reveals that the CCFE and SWIP schemes deliver similar results and exhibit better performance than the other IP methods for all quantities of interest.

TABLE 7. Errors of the solutions in L^2 norm of the CCFE method using Mesh 1 and 6 for the case of $\lambda_1 = 5.10^{-2}$ and $\lambda_1 = 5.10^{-3}$.

λ_1	Type of \mathfrak{T}_h	$err_{\mathfrak{T}_h}$	M
5.10^{-2}	Mesh 1	$8.76e - 4$	$2.93e - 5$
5.10^{-3}	Mesh 1	$2.40e - 2$	$1.30e - 1$
5.10^{-2}	Mesh 6	$1.90e - 3$	$2.69e - 7$
5.10^{-3}	Mesh 6	$3.17e - 2$	$6.87e - 2$

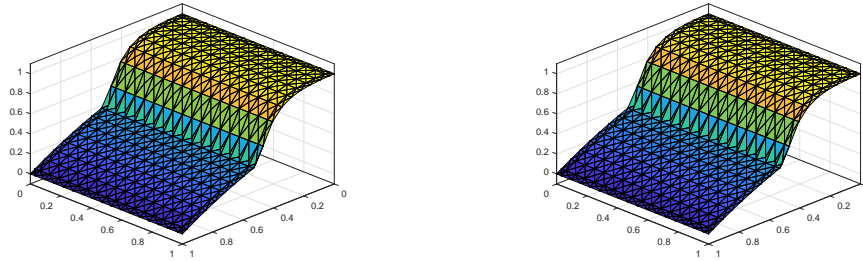


FIGURE 6. Graphical comparison of the exact solution u (left) and the numerical approximation u_h (right) obtained with the CCFE method in the test case 4.2, for $\lambda_1 = 0.1$, on Mesh 1 with mesh size $h = 0.0884$.

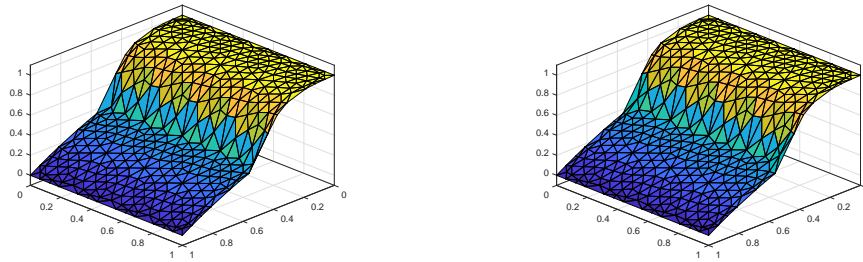


FIGURE 7. Graphical comparison of the exact solution u (left) and the numerical approximation u_h (right) obtained with the CCFE method in the test case 4.2, for $\lambda_1 = 0.1$, on Mesh 6 with mesh size $h = 0.1346$.

For $\lambda_1 = 0.1$ or 5.10^{-2} , Table 8 indicates that the maximum local Péclet numbers $Pe_{T_{max}}$ are less than 1 (except for $\lambda_1 = 5.10^{-2}$ on Mesh 6 with the mesh size $h = 0.1346$). In these non-convection-dominated regimes, we use the scheme as in (20) without the stabilization parameter δ_T . Consequently, the CCFE method on Meshes 1 and 6 performed well, as confirmed by the observations of the exact solution and the CCFE solution in Figures 6–9.

However, for $\lambda_1 = 5.10^{-3}$, the maximum local Péclet numbers $Pe_{T_{max}}$ are much greater than 1 (see Table 8), indicating a convection-dominated regime. In this case, the CCFE solution exhibits different behavior compared to the exact solution on the two meshes, as depicted in Figures 10 and 11. Specifically, it is lightly

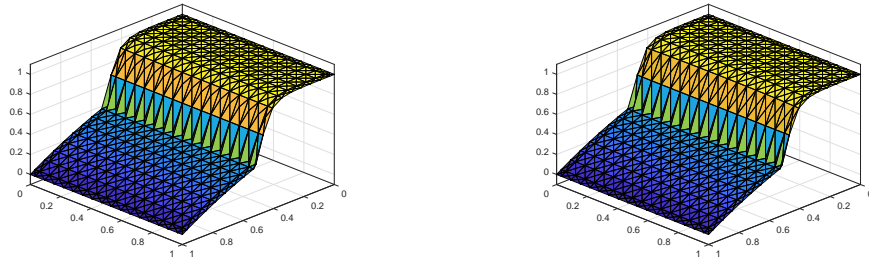


FIGURE 8. Graphical comparison of the exact solution u (left) and the numerical approximation u_h (right) obtained with the CCFE method in test case 4.2, for $\lambda_1 = 5.10^{-2}$, on Mesh 1 with mesh size $h = 0.0884$.

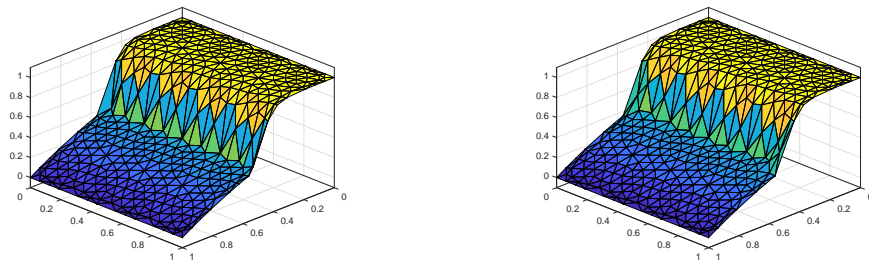


FIGURE 9. Graphical comparison of the exact solution u (left) and the numerical approximation u_h (right) obtained with the CCFE method in test case 4.2, for $\lambda_1 = 5.10^{-2}$, on Mesh 6 with mesh size $h = 0.1346$.

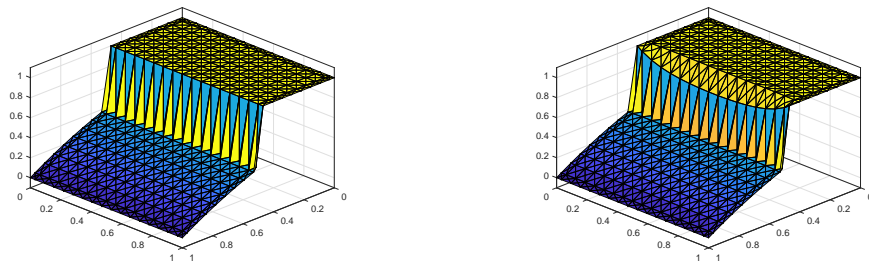


FIGURE 10. Graphical comparison of the exact solution u (left) and the numerical approximation u_h (right) obtained with the CCFE method in test case 4.2, for $\lambda_1 = 5.10^{-3}$, on Mesh 1, with mesh size $h = 0.0884$.

smearred at the internal layers on Mesh 1 (Figure 10), while on Mesh 6, minor overshooting occurs near the internal layer (Figure 11).

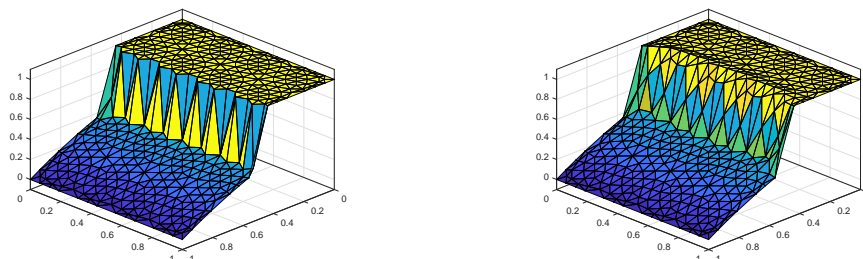


FIGURE 11. Graphical comparison of the exact solution u (left) and the numerical approximation u_h (right) obtained with the CCFE method in test case 4.2, for $\lambda_1 = 5.10^{-3}$, on Mesh 6, with mesh size $h = 0.1346$.

TABLE 8. Maximum local Péclet numbers $\text{Pe}_{T_{\max}}$ and associated stabilization parameters $\delta_{T_{\max}}$ in the test case 4.2.

λ_1	0.1	5.10^{-2}	5.10^{-3}	0.1	5.10^{-2}	5.10^{-3}
$\text{Pe}_{T_{\max}}$	$3.91e-1$	$7.81e-1$	$7.81e+0$	$7.71e-1$	$1.54e+0$	$1.54e+1$
$\delta_{T_{\max}}$	0	0	$3.41e-2$	0	0	$7.21e-2$
	Mesh 1, with mesh size $h = 0.0884$			Mesh 6, with mesh size $h = 0.1346$		

5. Conclusion

This paper proposes the CCFE scheme for the advection-diffusion problem considered with the heterogeneous and anisotropic diffusivities, and for the convection-dominated regime on general meshes. From a primal mesh, we can construct a dual mesh \mathfrak{T}_h^* and a triangular subdual mesh \mathfrak{T}_h^{**} . By these constructions, we approximate the solution of (3) by first-order polynomials on \mathfrak{T}_h^{**} . The degree of freedom of solution only includes primal cell-centred unknowns. Moreover, the above results in this study indicate that (i) it guarantees the local continuity of numerical fluxes, (ii) the method is presented within a rigorous theoretical framework to show coercive, strong & dual consistency and convergence properties, (iii) the numerical results showed that the proposed method converges with the expected rates of convergence, for heterogeneous and anisotropic diffusivities (possibly with discontinuous), and in convection-dominated regime on six types of primal meshes (in particular for heavily distorted meshes), and (iv) the method is easily implemented due to the conventional finite element codes on triangular meshes. However, a significant drawback of the proposed method is that it involves a stabilization parameter δ_T (see Eq. (21)), for which a general optimal choice has not yet been established. This can negatively impact the accuracy and convergence order of the method in specific cases, such as when dealing with a diffusion tensor exhibiting strong anisotropy that is nearly aligned with the mesh, and where diffusion is very weak in either the x -direction or y -direction. A further drawback of the proposed scheme is its inability to generalize to 3D convection-diffusion problems. To address this, we will study a scheme based on the enhanced flux continuity three-dimensional finite element method (EFC-3DFEM) proposed in [31]. This scheme

incorporates a streamline upwind diffusion term that utilizes discrete gradients. It also requires edge unknowns to ensure local flux continuity.

Acknowledgments

This research is funded by Vietnam National University Ho Chi Minh City (VNU-HCM) under grant number VL2023-18-01.

References

- [1] Christophe Potier and Hai Ong. A cell-centered scheme for heterogeneous anisotropic diffusion problems on general meshes. *Int. J. Finite Vol.*, 8:1–40, 2012.
- [2] S. Sun and J. Liu. A locally conservative finite element method based on piecewise constant enrichment of the continuous galerkin method. *Siam J. Sci. Compt*, 31:2528–2548, 2009.
- [3] Martin Stynes. Finite volume methods for convection-diffusion problems. *J. Comput. Appl. Math.*, 63:83–90, 1995.
- [4] R. Eymard, T. Gallouët, and R. Herbin. Finite volume methods. volume 7 of *Handbook of Numerical Analysis*, pages 713–1018. Elsevier.
- [5] I. Aavatsmark, T. Barkve, Ø. Bøe, and T. Mannseth. Discretization on unstructured grids for inhomogeneous, anisotropic media. Part I: Derivation of the methods. *SIAM J. Sci. Comp.*, 19:1700–1716, 1998.
- [6] I. Aavatsmark, T. Barkve, Ø. Bøe, and T. Mannseth. Discretization on unstructured grids for inhomogeneous, anisotropic media. Part II: Discussion and numerical results. *SIAM J. Sci. Comp.*, 19:1717–1736, 1998.
- [7] Enrico Bertolazzi and Gianmarco Manzini. A cell-centered second-order accurate finite volume method for convection-diffusion problems on unstructured meshes. *Math. Models Methods Appl. Sci.*, 14(8):1235–1260, 2004.
- [8] J. Droniou, R. Eymard, and R. Herbin. A unified approach to mimetic finite difference, hybrid finite volume and mixed finite volume methods. *Math. Models Methods Appl. Sci.*, 20:265–295, 2010.
- [9] B. D. Veiga, J. Droniou, and G. Manzini. A unified approach for handling convection terms in finite volumes and mimetic discretization methods for elliptic problems. *IMA J. Numer. Anal.*, 31:1357–1401, 2011.
- [10] J. Tinsley Oden, I. Babuška, and C. Erik Baumann. A discontinuous hp finite element method for diffusion problems. *J. Comput. Phys.*, 146:491–519, 1998.
- [11] B. Riviere. *Discontinuous Galerkin Methods for Solving Elliptic and Parabolic Equations: Theory and Implementation*. PA: SIAM, Philadelphia, 2008.
- [12] F. Brezzi, A. Buffa, and K. Lipnikov. Mimetic finite differences for elliptic problems. *Math. Model Numer. Anal.*, 43:277–295, 2009.
- [13] J. Droniou and R. Eymard. A mixed finite volume scheme for anisotropic diffusion problems on any grids. *Numer. Math.*, 105:35–71, 2006.
- [14] F. Hermeline. Benchmark on anisotropic problems: Numerical experiments with the DDFV method. In R. Eymard and J. Hérard, editors, *Finite Volumes for Complex Applications V*, pages 851–864, France, 2008. John Wiley & Sons.
- [15] Luca Gerardo-Giorda, Patrick Le Tallec, and Frédéric Nataf. A robin-robin preconditioner for advection-diffusion equations with discontinuous coefficients. *Comput. Methods Appl. Mech. Eng.*, 193(9 - 11), 2004.
- [16] Martin J. Gander and Tommaso Vanzan. Optimized schwarz methods for advection diffusion equations in bounded domains. In Kumar K. Berre I. Nordbotten J. Pop I. (eds) Radu, F., editor, *Numerical Mathematics and Advanced Applications ENUMATH 2017. Lecture Notes in Computational Science and Engineering*, vol 126. Springer, Cham., 2019.
- [17] H. G. Roos, M. Stynes, and L. Tobiska, editors. *Robust Numerical Methods for Singularly Perturbed Differential Equations: Convection-Diffusion-Reaction and Flow Problems*. Springer, Heidelberg, 2008.
- [18] C. Chainais-Hillairet and J. Droniou. Finite volume schemes for non-coercive elliptic problems with neumann boundary conditions. *IMA J. Numer. Anal.*, 31:61–85, 2009.
- [19] C. Dawson and V. Aizinger. Upwind-mixed methods for transport equations. *Comput. Geosci.*, 3:93–110, 1999.
- [20] J. Jaffre. Decentrage et elements finis mixtes pour les equations de diffusion-convection. *Calcolo*, 21:171–197, 1984.

- [21] Volker John and Petr Knobloch. On spurious oscillations at layers diminishing (SOLD) methods for convection-diffusion equations: Part I - A review. *Comput. Methods Appl. Mech. Engrg.*, 196:2197C2215, 2007.
- [22] A.N. Brooks and T.J.R. Hughes. Streamline upwind/ Petrov-galerkin formulations for convection dominated flows with particular emphasis on the incompressible Navier-Stokes equations. *Comput. Methods Appl. Mech. Engrg.*, 32, 1982.
- [23] Rajen K. Sinha and J. Geiser. Error estimates for finite volume element methods for convection-diffusion-creation equations. *Appl. Numer. Math.*, 57, 2007.
- [24] H. Vu, H. D. Nguyen, and T. H. Ong. A novel cell-centered approach of upwind types for convection diffusion equations on general meshes. *Int. J. Comput. Methods*, 18:235–256, 2021.
- [25] P. G. Ciarlet, editor. Basic error estimates for elliptic problems. *Handbook of numerical analysis (Ciarlet, P. G., Lions, J. L., eds.), vol. 2 : Finite-element methods (pt. 1)*, pp. 17C351, Amsterdam: North-Holland, 1991.
- [26] Volker John. *Finite element methods for incompressible flow problems*. Springer Series in Computational Mathematics, Berlin, 2016.
- [27] Tzon-Tzer Lu and Sheng-Hua Shiou. Inverse of 2×2 block matrices. *Comput. Math. Appl.*, 43:119–129, 2002.
- [28] J. Droniou, R. Eymard, T. Gallouet, and R. Herbin. Gradient schemes: A generic framework for the discretisation of linear, nonlinear and nonlocal elliptic and parabolic equations. *Math. Models Methods Appl. Sci.*, 23(13), 2013.
- [29] A. Ern, A. F. Stephansen, and P. Zunino. A discontinuous galerkin method with weighted averages for advection-diffusion equations with locally small and anisotropic diffusivity. *IMA J. Numer. Anal.*, pages 235–256, 2009.
- [30] Hanz Martin Cheng and Jan ten Thije Boonkkamp. A generalised complete flux scheme for anisotropic advection-diffusion equations. *Adv. Comput. Math.*, 47(19), 2021.
- [31] Ong Thanh Hai, Thi Hoai Thuong Nguyen, Anh Ha Le, and Nguyen Van Vuong Do. An enhanced flux continuity three-dimensional finite element method for heterogeneous and anisotropic diffusion problems on general meshes. *J. Engrg. Math.*, 145(16), 2024.

Department of Analysis, Faculty of Mathematics & Computer Science, University of Science, 227 Nguyen Van Cu, Ho Chi Minh, 700000, Vietnam.

Vietnam National University, Ho Chi Minh, 700000, Vietnam.

E-mail: othai@hcmus.edu.vn and hongthainguyenthi123@gmail.com

Department of Nuclear Physics, Faculty of Physics and Engineering Physics, University of Science, 227 Nguyen Van Cu, Ho Chi Minh, 700000, Vietnam.

Vietnam National University, Ho Chi Minh, 700000, Vietnam.

E-mail: ttthanh@hcmus.edu.vn